



## Insolation vs. meltwater control of productivity and sea surface conditions off SW Greenland during the Holocene

ESTELLE ALLAN , ANNE DE VERNAL , MARIT-SOLVEIG SEIDENKRANTZ , JASON P. BRINER, CLAUDE HILLAIRE-MARCEL , CHRISTOF PEARCE , LORENZ MEIRE , HANS RØY , ANDERS MØLLER MATHIASSEN, MIKKEL THY NIELSEN, JANE LUND PLESNER AND KERSTIN PERNER 

BOREAS



Allan, E., de Vernal, A., Seidenkrantz, M.-S., Briner, J. P., Hillaire-Marcel, C., Pearce, C., Meire, L., Røy, H., Mathiasen, A. M., Nielsen, M. T., Plesner, J. L. & Perner, K.: Insolation vs. meltwater control of productivity and sea surface conditions off SW Greenland during the Holocene. *Boreas*. <https://doi.org/10.1111/bor.12514>. ISSN 0300-9483.

We address here the specific timing and amplitude of sea-surface conditions and productivity changes off SW Greenland, northern Labrador Sea, in response to the high deglacial meltwater rates, the Early Holocene maximum insolation and Neoglacial cooling. Dinocyst assemblages from sediment cores collected off Nuuk were used to set up quantitative records of sea ice cover, seasonal sea-surface temperature (SST), salinity (SSS), and primary productivity, with a centennial to millennial scale resolution. Until ~10 ka BP, ice-proximal conditions are suggested by the quasi-exclusive dominance of heterotrophic taxa and low dinocyst concentrations. At about 10 ka BP, an increase in species diversity and abundance of phototrophic taxa marks the onset of interglacial conditions at a regional scale, with summer SST reaching up to 10 °C between 8 and 5 ka BP, thus in phase with the Holocene Thermal Maximum as recorded in the southern Greenlandic areas/northern Labrador Sea. During this interval, low SSS but high productivity prevailed in response to high meltwater discharge and nutrient inputs from the Greenland Ice Sheet. After ~5 ka BP, a decrease in phototrophic taxa marks a two-step cooling of surface waters. The first started at ~5 ka BP, and the second at ~3 ka BP, with a shift toward colder conditions and higher SSS suggesting reduced meltwater discharge during the Neoglacial. This second step coincides with the disappearance of the Saqqaq culture. The gap in human occupation in west Greenland, between the Dorset and the Norse settlements from 2000 to 1000 years BP, might be linked to high amplitude and high frequency variability of ocean and climate conditions.

*Estelle Allan (estelle.allan.56@gmail.com), Anne de Vernal and Claude Hillaire-Marcel, Centre de recherche sur la dynamique du système Terre (Geotop), Université du Québec à Montréal, C.P. 8888, succursale centre-Ville, Montréal, QC H3C 3P8, Canada; Marit-Solveig Seidenkrantz, Christof Pearce, Anders Møller Mathiasen, Mikkel Thy Nielsen and Jane Lund Plesner, Paleoceanography and Paleoclimate Group, Arctic Research Centre, and iClimate, Department of Geoscience, Aarhus University, Høegh-Guldbergs Gade 2, Aarhus DK-8000, Denmark; Jason P. Briner, Department of Geology, University at Buffalo, 411 Cooke Hall, Buffalo, NY 14260, USA; Lorenz Meire, Department of Estuarine and Delta Systems, Royal Netherlands Institute for Sea Research Utrecht University, Yerseke, The Netherlands and Greenland Climate Research Centre, Greenland Institute of Natural Resources, Nuuk 3900, Greenland; Hans Røy, Arctic Research Centre, Department of Biology, Aarhus University, Aarhus, Denmark, and Center for Geomicrobiology, Department of Biology, Aarhus University, Ny Munkegade 114-116, Aarhus DK-8000, Denmark; Kerstin Perner, Department of Marine Geology, Leibniz Institute for Baltic Sea Research, Seestrasse 15, Rostock 18119, Germany; received 26th May 2020, accepted 14th January 2021.*

In Arctic and sub-arctic areas, the ongoing climate change is accompanied by increased air and surface ocean temperatures, decreased sea ice cover, and enhanced ice-sheet melt (Golledge *et al.* 2019), especially along marine ice-sheet margins (Rignot *et al.* 2010; Hanna *et al.* 2013; Young & Briner 2015; Briner *et al.* 2016; Schweinsberg *et al.* 2018). Direct linkages between recent changes in the Greenland Ice Sheet (GrIS) mass balance and the strength of the Atlantic Meridional Overturning Circulation (AMOC) have been proposed (Rahmstorf *et al.* 2015; Jackson *et al.* 2016). Sévellec *et al.* (2017) hypothesized that a slowdown of the AMOC, related to enhanced Arctic freshwater export into the North Atlantic, would influence the global distribution of ocean temperature and thus the GrIS dynamics.

Since the Last Glacial Maximum, southwest Greenland has recorded a large reduction in ice volume with the ice margin retreating approximately 200 km from the continental shelf edge to its present inland position

(Lesnek *et al.* 2020; Young *et al.* 2020). Once off the shelf, GrIS retreat across the mainland seems to have occurred rapidly from *c.* 11.4 to 10.4 ka BP in the Nuuk region (Larsen *et al.* 2014, 2017). High summer insolation and temperatures during the Early and Middle Holocene lasted until about 5 ka BP (Briner *et al.* 2016) and resulted in a simulated GrIS ice mass loss rate of about 100 Gt a<sup>-1</sup> (Lecavalier *et al.* 2014; Larsen *et al.* 2015; Cuzzone *et al.* 2019). The Late Holocene experienced a cooling related to reduced summer insolation that presumably favoured the growth of the GrIS, ice caps and local glaciers since about 4000 years ago (Funder *et al.* 2011; Briner *et al.* 2016; Larsen *et al.* 2017; Schweinsberg *et al.* 2018).

Sediment archives along the West Greenland coastal and shelf area are ideally located to document freshwater fluxes from the melting GrIS, thus providing clues on ocean-ice dynamics and GrIS history. Today, the West Greenland margin is bathed by the West Greenland

Current (WGC; Fig. 1), which results from the mixing of warm and saline waters of the Irminger Current (IC; Fig. 1) with cold and low salinity waters of the East Greenland Current (EGC; Fig. 1) (e.g. Buch 1981; Tang *et al.* 2004). Along the West Greenland coast, land-terminating and tidewater glaciers characterize the margin of the GrIS, including three tidewater outlet glaciers, the Kangiata Nunaata Sermia (KNS), Akullersuup Sermia (AS) and Narsap Sermia (NS), in Godthåbsfjord (Fig. 1; Mortensen *et al.* 2014; Pearce *et al.* 2018). Such marine-terminating glaciers induce high primary productivity by meltwater discharge at the base of tidal glaciers contributing to vertical mixing in the water column and nutrient resuspension towards the surface (Boertmann *et al.* 2013; Juul-Pedersen *et al.* 2015; Meire *et al.* 2017). Hence, the meltwater runoff from the GrIS causes a second algal bloom that occurs in summer–autumn, after the spring bloom (Juul-Pedersen *et al.* 2015; Krawczyk *et al.* 2015, 2018; Meire *et al.* 2016).

Ocean conditions during the Holocene have been well documented for selected regions off West Greenland, in

particular in the Disko Bay area (Fig. 1), where a number of sedimentological, micropalaeontological and geochemical investigations have been conducted (Moros *et al.* 2006, 2016; Lloyd *et al.* 2007; Seidenkrantz *et al.* 2008; Krawczyk *et al.* 2010, 2013, 2017; Andresen *et al.* 2011; Perner *et al.* 2011, 2013; Ribeiro *et al.* 2012; Jennings *et al.* 2014; Ouellet-Bernier *et al.* 2014; Sha *et al.* 2014; Kolling *et al.* 2017; Allan *et al.* 2018). The records from the aforementioned studies have shown a relatively late establishment of the Holocene Thermal Maximum (HTM) following the phase of maximum insolation in the Early Holocene in surface waters, and a decoupling between surface and subsurface temperatures during the Middle Holocene, which presumably link to meltwater discharge from the GrIS and the history of the relatively warm WGC (Moros *et al.* 2016). In the Disko Bay area, full interglacial conditions in surface waters became established at  $\sim 7.5$  to  $\sim 7.3$  ka BP and lasted until the general cooling started at about  $\sim 4$  ka BP (Jennings *et al.* 2014; Ouellet-Bernier *et al.* 2014; Moros *et al.* 2016). A comparable timing for a general shift in

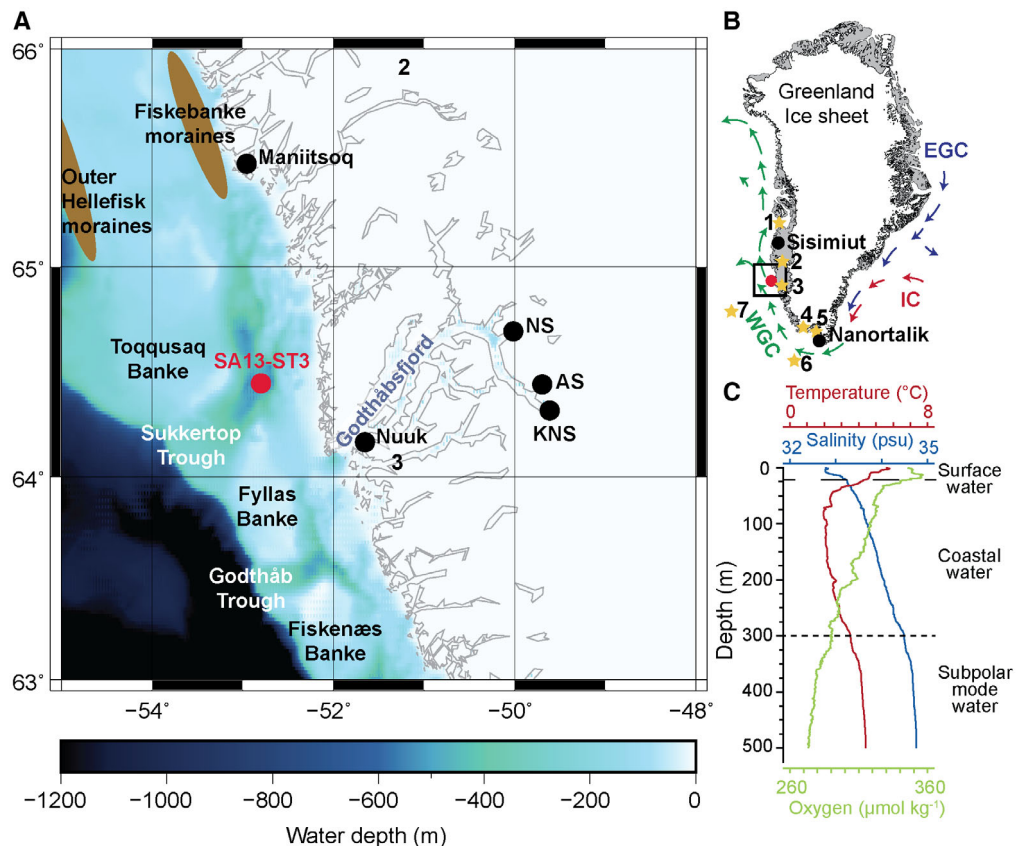


**Fig. 1.** A. Map of the study area. The red dots indicate the location of the coring site SA13-ST3. Acronyms of the tidewater outlet glaciers: KNS = Kangiata Nunaata Sermia; AS = Akullersuup Sermia; NS = Narsap Sermia. B. The dominant ocean circulation pattern around Greenland: EGC = East Greenland Current; IC = Irminger Current; WGC = West Greenland Current. The yellow stars indicate the location of cores referred to in the text: 1 = Disko Bugt (Perner *et al.* 2013; Ouellet-Bernier *et al.* 2014; Moros *et al.* 2016; Allan *et al.* 2018); 2 = Sukkertoppen ice cap area (Schweinsberg *et al.* 2018); 3 = Ameralik fjord (Seidenkrantz *et al.* 2007); 4 = Qipisarqo Lake (Fr chet & de Vernal 2009); 5 = Narsaq Sound (N rgaard-Pedersen & Mikkelsen 2009); 6 = Greenland Rise (Solignac *et al.* 2004); 7 = northwest Labrador Sea (Gibb *et al.* 2014, 2015). C. CTD profile from site SA13-ST3 (SA13-ST3-19CTD) obtained August 2013 (Seidenkrantz *et al.* 2013b).

hydrographic conditions has also been documented for Ameralik fjord just south of Nuuk (Ren *et al.* 2009; Seidenkrantz *et al.* 2013a). During the Late Holocene, alternating cold (3.5 to 2.7 ka BP) and milder (2.7 to 1.2 ka BP) conditions were recorded regionally and were tentatively related to variations in meltwater discharge and advances of tidewater glaciers along the West Greenland margin (Moros *et al.* 2016). Studies from the Ameralik fjord in the Godthåbsfjord system (Møller *et al.* 2006; Seidenkrantz *et al.* 2007) and Narsaq Sound, South Greenland (Nørgaard-Pedersen & Mikkelsen 2009), indicated that recent variations of Atlantic water inflow into the fjords followed a long-term North Atlantic Oscillation (NAO) pattern (Møller *et al.* 2006; Seidenkrantz *et al.* 2007; Nørgaard-Pedersen & Mikkelsen 2009). However, while these results have a local significance, their implications for the regional oceanography need to be fully documented. The study of cores HU2008-029-04 and HU2008-029-70 from the northern Labrador Sea permitted the reconstruction of low surface salinities from the Lateglacial to the Late to Middle Holocene in the central Labrador Sea, suggesting linkages between sea-surface salinity, ice-sheet retreat and meltwater release (Gibb *et al.* 2015).

In order to better describe the climate–ice–ocean interactions along the southwest Greenland margin during the Holocene, we investigated a series of marine sediment cores from station SA13-ST3, off Nuuk (Seidenkrantz *et al.* 2013b). This site is located on the West Greenland shelf allowing us to identify variations in freshwater fluxes from the southern GrIS. The nearby Rumohr lot cores SA13-ST3-15R and SA13-ST3-16R allow comparison to modern and sub-recent conditions. Here, we present the results from palynological analyses of these cores, with special attention paid to the distribution of dinoflagellate cysts (hereafter dinocysts), which we used to reconstruct sea-surface conditions including sea-surface temperature (SST) and salinity (SSS). In addition, we present isotopic data from benthic foraminifers, geochemical and XRF data with the objective to decipher sea-surface conditions from bottom-water properties that are influenced by Atlantic and polar water masses from the WGC, coastal currents and local meltwater supply. We also compare our results to previously published palaeoceanographic records (Fig. 1) from the Disko Bay (Perner *et al.* 2013; Ouellet-Bernier *et al.* 2014; Moros *et al.* 2016; Allan *et al.* 2018), Ameralik fjord (Seidenkrantz *et al.* 2007), West Greenland region (Larsen *et al.* 2017; Levy *et al.* 2017; Schweinsberg *et al.* 2017, 2018) and the northwest Labrador Sea (Gibb *et al.* 2014, 2015; Fig. 1), in order to assess the regional significance of our data.

## Regional setting

Site SA13-ST3 (latitude 64°26.7425'N, longitude 52°47.6486'W) is located off the Godthåbsfjord (Nuup

Kangerlua) system in the Sukkertop Trough between Toqqusaq Banke and Fyllas Banke, where the water depth ranges from 200 to 600 m (Fig. 1). The Sukkertop Trough, formed by an ice stream under full glacial conditions, experienced rapid and episodic delivery of glacial sediments during the retreat of the ice margin after the Last Glacial Maximum (Dowdeswell *et al.* 2016; Ryan *et al.* 2016).

At present, the West Greenland Current (WGC) flows northwards on the West Greenland shelf where Subpolar Mode Water (SPMW) occupies the water column from ~300 m down to the bottom of the Sukkertop Trough (Fig. 1C; Rysgaard *et al.* 2020). The WGC is formed from the warm and saline waters of the Irminger Current (IC), which is a side branch of the North Atlantic Current mixing with fresh and cold waters carried by the East Greenland Current (EGC) (Tang *et al.* 2004; Ribergaard 2014; Fig. 1). The upper water layer is characterized by coastal water (CW), a water mass with lower salinity (31.9–32.9 psu) and temperatures, which is the last stage of the transformation of Polar Surface Water. The low-salinity surface waters form a thin mixed layer of about 20 m above a sharp pycnocline (Fig. 1). It is marked by low thermal inertia and summer warming with summer SST ranging from 4.0–5.2 °C (Ribergaard 2014). At the sampling site, in August 2013, SSS ranged from 32.8 at the surface to 34.8 psu at the bottom (Fig. 1). Satellite data suggest high summer primary production with average rates of  $895 \pm 51 \text{ mg C m}^{-2} \text{ d}^{-1}$ . In winter, the West Greenland shelf including the Godthåbsfjord at the vicinity of the study site is generally sea-ice free whereas the inner fjords freeze over from November to April–May (Mortensen *et al.* 2011).

## Material and methods

### Data and sample collection

All data and samples from station SA13-ST3 were collected on the shelf off the Godthåbsfjord complex in August 2013 during a cruise of the RV 'Sanna' (Seidenkrantz *et al.* 2013b).

During the cruise, a conductivity-temperature-depth profile (at 64°26.7574'N, 52°46.7231'W, water depth 518.9 m) was collected using a Seabird SBE19+ (Fig. 1). Several cores were collected at the site. They include a gravity core 20G (SA13-ST3-20G; 64°26.7425'N, 52°47.6486'W, water depth 498 m, core length 587 cm), Rumohr lot core 16R (SA13-ST3-16R; 64°27.0694'N, 52°47.5783'W, water depth 475 m, core length 52 cm) and Rumohr lot core 15R (SA13-ST3-15R; 64°26.8855'N, 52°47.6544'W water depth 495.5 m; core length 53.5 cm). Rumohr lot cores 15R and 16R were recovered with an intact sediment surface and without suspended material in the water above the core. This indicates that there was no loss of material from the surface during coring. The sediment pore-water geochemistry indicates

that the cores overlap, with the upper 18 cm of sediment in the Rumohr lot core 16R missing from the gravity core (Pelikan *et al.* 2019). Microbiological and geochemical data have been presented by Glombitza *et al.* (2015), Braun *et al.* (2017) and Pelikan *et al.* (2019).

#### <sup>210</sup>Pb measurement in Rumohr lot core 15R

In the 52-cm-long Rumohr lot core 15R, which contained no biogenic remains allowing direct <sup>14</sup>C dating, we analysed <sup>210</sup>Pb at Geotop-UQAM (Montreal, Canada). The <sup>210</sup>Pb activities were obtained indirectly by measuring the decay rate of its daughter isotope <sup>210</sup>Po (t<sub>1/2</sub> 5 138.4 d; α = 5.30 MeV) in alpha spectrometry. A <sup>209</sup>Po spike was added to the samples to determine the extraction and counting efficiency. Polonium was extracted from dried and crushed sediments and purified by chemical treatments with hydrochloric acid, nitric acid, hydrofluoric acid, and peroxide, prior to deposition on a silver disc. The <sup>209</sup>Po and <sup>210</sup>Po activities were measured in a silicon surface-barrier multichannel a-spectrometer (EGG-ORTEC type 576A). Uncertainties were estimated to be ±2–4% (one standard

deviation). Results are reported in Table S1. The age model of 16R is provided by Krawczyk *et al.* (2021).

#### Age model of gravity core 20G

In the gravity core 20G, the chronological framework is based on 32 AMS <sup>14</sup>C dates of mixed benthic foraminifers and mollusc shells in addition to two samples of macroalgae remains (Table 1). The samples were analysed at the accelerator mass spectrometry (AMS) facilities in Zurich, Ottawa and Aarhus (ETH, UOC, AAR). All the radiocarbon dates were calibrated using the Marine13 calibration curve and a marine reservoir correction with ΔR of 140±35 years (Reimer & Reimer 2001; Lloyd *et al.* 2011; Moros *et al.* 2016). The age-depth model was constructed using OxCAL v4.3.2 (Bronk Ramsey 2008, 2009) and a Poisson-process deposition model for the core interval contained between 62.5 and 514 cm, from the oldest to the youngest radiocarbon date (Table 1). Above and below these levels, due to the lack of dateable material, linear extrapolations were applied assuming a constant sedimentation rate (Fig. 2). All dates were in good agreement except for one radiocarbon date at 321 cm, which may be slightly too young relative

Table 1. Radiocarbon dates and calibrated ages from core SA13-ST3-20G.

Depth (cm)	Lab. code	Material dated	Radiocarbon age (a BP)	Error (a)	Calibrated 2σ (95.4%) age range (cal. a BP)	Modelled median age (cal. a BP)
62.5	ETH-67565	Mixed benthic foraminifers	1460	55	712–1001	728
80.5	ETH-67566	Mixed benthic foraminifers	1425	75	665–989	897
101.5	ETH-67567	Mixed benthic foraminifers	1735	65	980–1286	1127
110.5	UOC-2531	Organic	1791	25	1104–1295	1216
124.5	ETH-81613	Mixed benthic foraminifers	1890	45	1175–1418	1333
129.5	UOC-2532	Organic	1958	30	1274–1485	1384
150.5	ETH-67568	Mixed benthic foraminifers	2240	60	1521–1852	1681
163.5	AAR-20067	Mollusc shell	2362	25	1704–1932	1855
172.5	ETH-81614	Mixed benthic foraminifers	2480	45	1821–2111	2025
189.5	ETH-87319	Mixed benthic foraminifers	2975	50	2395–2732	2542
198.5	ETH-81615	Mixed benthic foraminifers	3110	50	2601–2911	2745
218.5	ETH-67569	Mixed benthic foraminifers	3370	65	2837–3249	3154
238.5	ETH-81616	Mixed benthic foraminifers	3935	50	3570–3900	3771
259.5	ETH-81617	Mixed benthic foraminifers	4550	50	4415–4776	4545
283.5	ETH-67570	Mixed benthic foraminifers	5150	70	5134–5568	5259
303.5	ETH-87320	Mixed benthic foraminifers	5300	60	5324–5648	5594
318.5	ETH-67571	Mixed benthic foraminifers	5880	65	5961–6296	6102
321.0	UOC-2330	Mollusc shell	5612	30	5719–5950	n.a. (outlier)
330.5	ETH-94446	Mixed benthic foraminifers	6095	60	6231–6539	6386
346.0	AAR-20068	Mollusc shell	6446	30	6646–6889	6789
366.5	ETH-81618	Mixed benthic foraminifers	7145	60	7385–7625	7535
375.5	ETH-94447	Mixed benthic foraminifers	7880	65	8030–8355	8200
380.5	ETH-87321	Mixed benthic foraminifers	8180	70	8340–8710	8438
387.5	ETH-67572	Mixed benthic foraminifers	8315	75	8465–8950	8627
410.5	ETH-87322	Mixed benthic foraminifers	8755	70	9055–9450	9185
428.5	ETH-67573	Mixed benthic foraminifers	9120	85	9456–9993	9524
435.0	AAR-20069	Mollusc shell	9033	40	9444–9685	9601
451.5	ETH-94448	Mixed benthic foraminifers	9235	70	9577–10 110	9884
463.5	ETH-87323	Mixed benthic foraminifers	9480	70	9919–10 381	10 118
478.5	ETH-67574	Mixed benthic foraminifers	9725	75	10 236–10 651	10 321
495.5	ETH-94449	Mixed benthic foraminifers	9725	75	10 236–10 651	10 523
514.0	AAR-20070	Mollusc shell	9868	40	10 490–10 786	10 757

to its position in the stratigraphy, possibly due to burrowing of the dated mollusc below the sediment surface. Dates indicate that the core covers the entire Holocene.

#### XRF core scanning and magnetic susceptibility

The qualitative geochemical content in the sediment cores was measured on split halves of cores 20G and 16R using an ITRAX X-ray fluorescence (XRF) core scanner

(Croudace *et al.* 2006) equipped with a Molybdenum tube at the Department of Geoscience, Aarhus University, Denmark. Measurements were carried out at 30 kv and 40 mA at 1-mm intervals for 10 s. We subsequently combined data at 2-mm intervals to reduce noise. Here, we report semi-quantitative abundance data for iron (Fe), titanium (Ti) and calcium (Ca), measured as counts per second (cps). Values of Fe and Ti and the ratio of Fe/Ca (all in cps) are used as indicators of terrestrial inputs. Data are reported in Table S2. The magnetic suscepti-

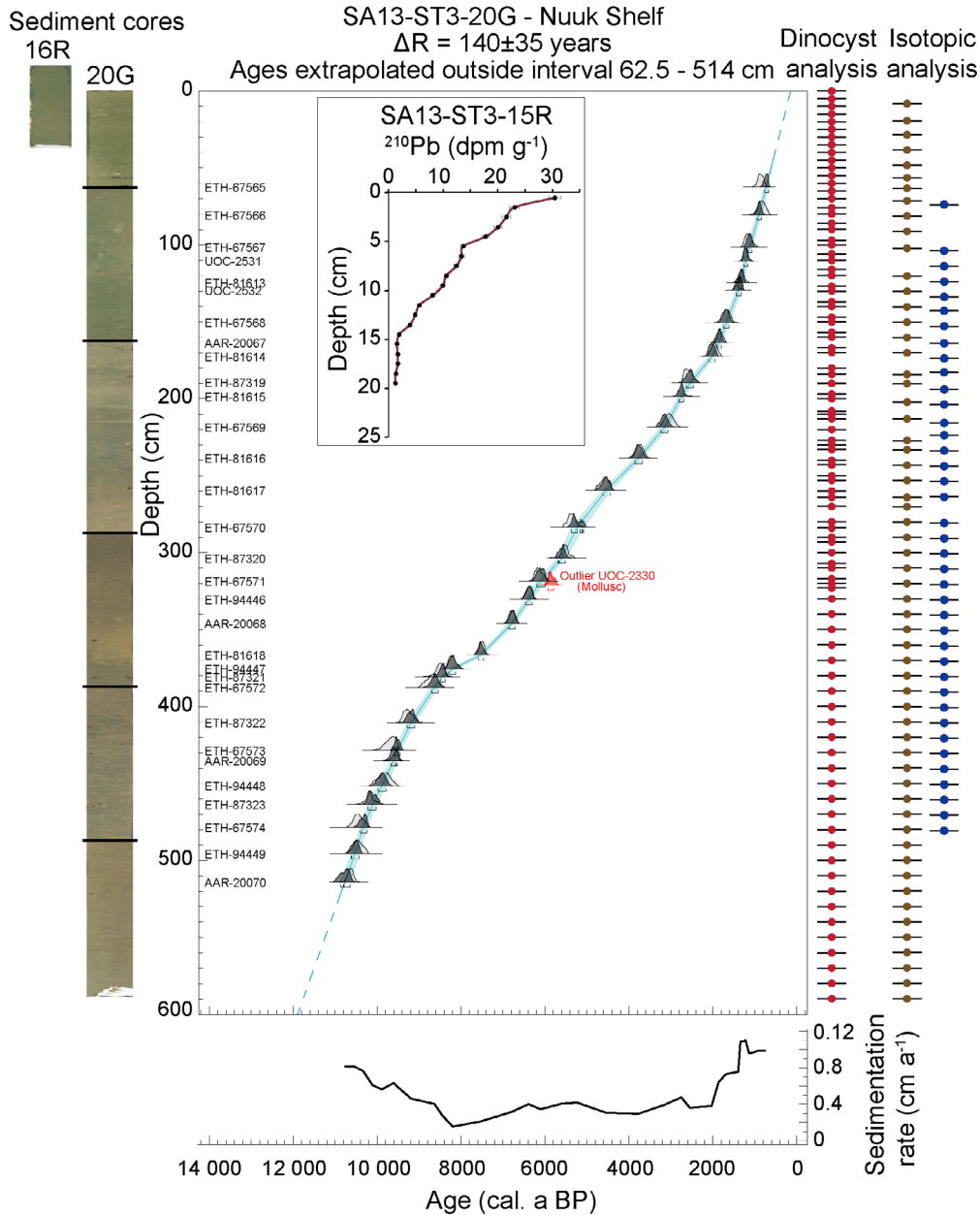


Fig. 2. Combined ITRAX line scan images of the sediment core sections and age-depth relationship for cores SA13-ST3-20G and SA13-ST3-16R; the slight colour changes between sections are due to camera calibration issues. The blue shaded area displays the age-depth uncertainty. The bars on the right show the depth of samples used for palynological analysis (red dots) and the stable isotope analysis of organic matter (brown dots) and benthic foraminifers (blue dots) in the core SA13-ST3-20G in depth.

bility (MS) was also measured on the split halves of the cores using a Bartington MS2E meter with a resolution of 5 mm on the ITRAX core scanner. Results are reported in Table S2. Prior to these measurements, a line scan image was produced for each core section using the ITRAX.

#### *Calcium carbonate and organic carbon content*

The calcium carbonate ( $\text{CaCO}_3$ ) and organic carbon ( $\text{C}_{\text{org}}$ ) contents of core 20G were measured at the Department of Geosciences and Natural Resource Management, University of Copenhagen, Denmark. Analyses were carried out every 5 to 10 cm on dried samples. First, total carbon was measured using an Eltra CS-500 analyser. An approximately 0.25-g sample was weighed into a ceramic combustion boat and burned in the furnace at 1350 °C. The instrument was calibrated using a standard containing 5% C. Subsequently,  $\text{CaCO}_3$  was measured on a Metrohm 855 Robotic Titrosampler. An approximately 1.0-g sample was weighed into a 150 mL beaker; 15 mL of 1.0 M HCl plus ~100 mL demineralized water was added. The mixture was boiled on a hotplate for 20 min. and then titrated with 1.0 M sodium hydroxide (NaOH) until neutral pH (7) was reached. The instrument accuracy was checked using pure  $\text{CaCO}_3$  (100%) and the electrode was calibrated with buffer pH 4, 7 and 9. Finally, the total organic carbon (TOC) was calculated using this formula:

$$\text{TOC}\% = \text{TC}\% - \frac{\text{CaCO}_3\% \times 12.01 \frac{\text{g}}{\text{mol}} \text{C}}{100.08 \frac{\text{g}}{\text{mol}} \text{CaCO}_2} \quad (1)$$

Data are reported as weight % of the dry sediment.

#### *Particle size analysis*

Grain-size distribution was measured on 119 samples from core 20G at the Department of Geoscience, Aarhus University using a Sympatec Helos laser diffractometer using an R4 lens for the fraction <63  $\mu\text{m}$  and an R7 lens for the 63  $\mu\text{m}$ –2 mm fraction. The size distribution was grouped into three fractions: sand (>60  $\mu\text{m}$ ), silt (2–60  $\mu\text{m}$ ) and clay (<2  $\mu\text{m}$ ). Here, we have used the >60  $\mu\text{m}$  fraction as an indicator of ice-rafted deposition. Data are reported in Table S3.

#### *Stable oxygen and carbon isotope analysis*

Oxygen and carbon isotope compositions ( $\delta^{18}\text{O}$ ,  $\delta^{13}\text{C}$ ) of the deep benthic foraminiferal species *Nonionellina labradorica* (Dawson), common throughout most of the studied sequence, were determined at Geotop-UQAM. Approximately 100  $\mu\text{g}$  (between 25 and 65 specimens from the >100  $\mu\text{m}$  fraction) were heated at 90 °C for 1 h before analysis with an isotope ratio mass

spectrometer (Micromass-Isoprime™) coupled to a MultiCarb™ system in dual inlet mode. Because isotope values of the samples are expected to be close to our home standard UQ6 ( $\delta^{13}\text{C} = 2.21 \pm 0.03\text{‰}$ ;  $\delta^{18}\text{O} = -1.48 \pm 0.03\text{‰}$ ), calibrated using NBS19 & LSVEC (Assonov *et al.* 2020), only UQ6 was used to normalize the results on the VPDB scale. The overall analytical uncertainty ( $\pm 1\sigma$ ) propagated to the VPDB scale is better than  $\pm 0.05\text{‰}$  for  $\delta^{13}\text{C}$  and  $\pm 0.08\text{‰}$  for  $\delta^{18}\text{O}$ . Results are reported in Table S4.

The carbon isotope composition ( $\delta^{13}\text{C}$ ) of the organic matter was determined at Geotop-UQAM. The samples were weighted in tin cups and steam treated with HCl (36%) for 24 h to eliminate the carbonate fraction before analysis with an isotope ratio mass spectrometer (Micromass-Isoprime™) coupled to an Elementar Vario Micro-Cube elemental analyser in continuous flow mode. Two internal reference materials ( $\delta^{13}\text{C} = -28.73 \pm 0.06$  and  $-11.85 \pm 0.04\text{‰}$ ) were used to normalize the results on the NBS19-LSVEC scale. A third reference material ( $\delta^{13}\text{C} = -17.04 \pm 0.11\text{‰}$ ) was analysed as an unknown to assess the exactness of the normalization. The overall analytical uncertainty ( $\pm 1\sigma$ ) propagated to the VPDB scale is better than  $\pm 0.1\text{‰}$ . Results are reported in Table S4.

#### *Palynological analyses*

In this study, 105 samples were analysed for their palynological content. A total of 14 samples are from Rumohr lot core 16R and 91 samples from gravity core 20G. The Rumohr lot core 16R was analysed at 4-cm intervals and the gravity core 20G at 3 to 7 cm in the upper 330 cm and every 10 cm to the bottom (Fig. 2), which gives a centennial temporal resolution.

Volumes of 3–5  $\text{cm}^3$  of sediment were prepared at Geotop-UQAM following the protocol described by de Vernal *et al.* (1996). After wet sieving, the 10–106  $\mu\text{m}$  fraction of each sample was treated with cold HCl (10%) and HF (50%) to dissolve carbonate and silicate particles, respectively. Tablets with known amount of *Lycopodium* spores were added to allow calculation of the concentrations of palynomorphs. The overall uncertainty of the calculated concentrations includes the error in the number of marker grains added and counted and the error in palynomorph counts, in addition to the uncertainty in the sedimentation rate (e.g. Mertens *et al.* 2009). In order to avoid these issues, we refer mostly results by the first order estimates and by their magnitudes. The final residue was mounted on microscope slides with glycerine jelly for further observation with a transmitted light microscope at 400 to 1000 $\times$  magnification. All palynomorphs were counted including dinocysts, which were identified to the species level, organic linings of benthic foraminifers, *Halodinium* spp., pollen grains and spores of pteridophytes and bryophytes, which were identified at the genus or family level.

At least 300 specimens of dinocysts were identified and counted in each sample, which provides statistically reliable counts (e.g. Mertens *et al.* 2009). The taxonomic nomenclature of dinocysts is based on Rochon *et al.* (1999) and Radi *et al.* (2013) and conform to the updated by Van Nieuwenhove *et al.* (2020). Here we report mostly on dinocyst assemblages and detailed results can be found in Table S5.

#### Statistical data treatments

Multivariate analyses (detrended correspondence analysis and principal component analysis) were performed on dinocyst data using the CANOCO 5 software (ter Braak & Šmilauer 2012; Lepš & Šmilauer 2014) in order to represent graphically the major patterns in the relationship between taxa in the assemblages of cores 20G and 16R (Legendre & Birks 2012). To reduce the effect of dominant species and closed-sum percentage data, the Shapiro & Wilks (1965) statistical test for normality was performed (Legendre & Legendre 2012). A logarithmic transformation was applied to dinocyst data reported as percentages to emphasize the weight of accompanying taxa. The occasional occurrences were discarded and only the taxa recording more than 1% in at least one sample and occurring in more than three samples were used for statistical analyses. Here, detrended correspondence analysis performed on dinocyst assemblages showed the length of the first ordination axis to be 1.8 standard deviations, which suggests a linear relationship and that principal component analysis (PCA) is appropriate (ter Braak & Šmilauer 1998).

The modern analogue technique (MAT) was applied to dinocyst assemblages in order to reconstruct sea-surface parameters (de Vernal *et al.* 2001, 2013) using the updated reference database of the Northern Hemisphere that includes 1968 reference sites (de Vernal *et al.* 2020). Several methodological approaches have been developed to reconstruct climate and ocean parameters from microfossil assemblages (e.g. Guiot & de Vernal 2007). Among them, MAT, which relies on the similarities between fossil and modern assemblages instead of using mathematical relationships or calibrations to infer oceanographic conditions, is the most frequently applied technique for dinocyst data. Trials with techniques using calibrations such as the artificial neural network (ANN) and the weighted averaging partial least square (WA-PLS) have been done (Peyron & de Vernal 2001; Bonnet *et al.* 2010; Guiot & de Vernal 2011; Hohmann *et al.* 2020). ANN and WA-PLS may perform almost as well as MAT, but the geographical domain (regional or hemispheric) used for the calibration data set leads to different results. For this reason, with the aim to provide as objective as possible reconstruction results, we used MAT applied to the updated modern dinocyst database of the Northern Hemisphere. Moreover, MAT permits simultaneous reconstruction of more than one param-

eter (e.g. Guiot & de Vernal 2007). Although it can be a matter of debate as the biological data explain only a small number of independent parameters in the environment (Juggins & Birks 2012; Juggins 2013). Here, we reconstruct four surface ocean parameters: summer temperature, salinity and productivity in addition to the seasonal duration of sea ice cover. Multivariate analyses of recent dinocyst assemblages from the Northern Hemisphere show that the temperature, salinity, productivity and the seasonal duration of sea ice cover explain a large part of the dinocyst assemblage distribution as defined from the first three axes of canonical correspondence analyses (de Vernal *et al.* 2020). Statistical analyses of Atlantic-Arctic and Pacific data sets also indicated that the dinocyst distribution is controlled by independent oceanographic parameters, which may however differ from one region to another (cf. Hohmann *et al.* 2020). Therefore, whereas multiple parameters can be theoretically reconstructed from dinocyst data, including salinity, temperature, sea ice and productivity, the most appropriate variables for reconstructions are not necessarily unequivocal. Hence, caution is needed when using and interpreting the quantitative estimates of past sea-surface conditions.

The MAT was performed using the 'bioindic' package developed by Guiot for the R platform (<http://cran.r-project.org/>) and following the procedures described by de Vernal *et al.* (2013). For reconstructions, we proceeded with searches of five analogues after logarithmic transformation of the relative taxa abundances. The best estimates were calculated from the mean of the corresponding sea-surface values weighted according to the similarity of the analogues. The use of weighted averages may result in smoothing but taking into consideration the five best analogues illustrates the full range of hydrographic values possible. The Northern Hemisphere dinocyst database we used includes 71 taxa and 1968 reference sites from coastal, estuarine and open ocean settings. It thus represents a wide range of sea-surface salinity (5 to 38 psu), temperature (−1.8 to 30 °C), sea ice cover (0–12 months a<sup>−1</sup>) and productivity (up to 12 000 µg C m<sup>−2</sup> d<sup>−1</sup>) (de Vernal *et al.* 2020). The errors of predictions were calculated by comparing the best estimated values with the measurements at sample sites. They are as follows: 1.5 months a<sup>−1</sup> for sea ice cover, 719 mg C m<sup>−2</sup> d<sup>−1</sup> for summer primary productivity, 1.75 °C for summer temperature and 2.04 psu for summer salinity. Results are summarized here and detailed in Table S5.

## Results

### Chronology

The calibrated <sup>14</sup>C ages indicate that the gravity core 20G encompasses at least the last 11 000 years (Fig. 2). The mean sedimentation rates are approximately 0.06 cm a<sup>−1</sup>

throughout the sequence, with an average of  $0.1 \text{ cm a}^{-1}$  over the last 1500 years,  $0.04 \text{ cm a}^{-1}$  from 9000 to 1500 years ago and  $0.08 \text{ cm a}^{-1}$  from *c.* 10 700 to 9000 years ago (Fig. 2), which permits palaeoclimatic reconstructions to be resolved at centennial to millennial time scales. Despite the loss of about 18 cm of sediment at the top of the core, the gravity core sufficiently overlaps with Rumohr lot core 16R (Pelikan *et al.* 2019) to encompass a complete Holocene sequence. In this paper we report results in calibrated kilo-years (ka) BP.

$^{210}\text{Pb}$ -excesses were observed down to  $\sim 15 \text{ cm}$  in core 15R (Fig. 2; Table S1) and the high  $^{210}\text{Pb}$  activity throughout the core confirmed that modern sediment was recovered at the surface (cf. Smith & Schafer, 1984). The slight offset between recent sedimentation rates estimated from  $^{14}\text{C}$  data ( $>1 \text{ mm a}^{-1}$ ) vs. the depth penetration of  $^{210}\text{Pb}$ -excesses ( $\sim 15 \text{ cm}$ ) accumulated over the last 100 years may be due to benthic mixing. The increased water content towards the top of the core may have induced an apparent increase in sedimentation rates, which could explain the slight  $^{14}\text{C}$  vs.  $^{210}\text{Pb}$  time-offset. Unfortunately, the lack of precise density measurements prevents the estimation of more robust accumulation rate estimates from core 15R (i.e. in  $\text{g cm}^{-2} \text{ a}^{-1}$ ) prevents a robust calculation of the age model of core 15R; consequently all data from cores 15R and 16R are shown vs. depth (e.g. Figs 3, 4). Matching XRF and magnetic susceptibility results from the gravity

and the Rumohr lot cores from the site SA13-ST3 supports the age model from the gravity core 20G (Fig. 3).

#### Geochemical data

Concentrations of iron (Fe) and titanium (Ti) based on XRF measurements show similar patterns. A rapid decrease in both Fe and Ti concentrations is recorded from the core-bottom up to the  $\sim 10 \text{ ka BP}$  dated layer. This is followed by their continuous increase towards the core-top, up to the last 10 cm of Rumohr lot core 16R, marked by a reverse trend (Fig. 3). High concentrations of Fe and Ti suggest high terrestrial inputs as they both derive from the siliciclastic fraction of continental material (Rothwell & Croudace 2015). In the study area, they can be related to runoff, meltwater discharge or ice-rafting (e.g. St-Onge *et al.* 2007; Solignac *et al.* 2011; Pearce *et al.* 2014). The calcium carbonate ( $\text{CaCO}_3$ ) content of the sediment ranges from  $\sim 1.4$  to  $\sim 14.2\%$  (Fig. 3). It shows variations opposite to those of Fe and Ti, but parallel to those of Ca/Fe. This suggests that  $\text{CaCO}_3$  fluctuations are mostly driven by variations in the sedimentation of biogenic carbonate (foraminifers and coccoliths). Weight percentages of  $\text{C}_{\text{org}}$  range from  $\sim 0.02$  to  $\sim 2.4\%$  (Fig. 3).  $\text{C}_{\text{org}}$  and  $\text{CaCO}_3$  show different trends. The  $\text{C}_{\text{org}}$  recorded a steady increase from  $\sim 0.02\%$  at the bottom of the core to reach maximum values of

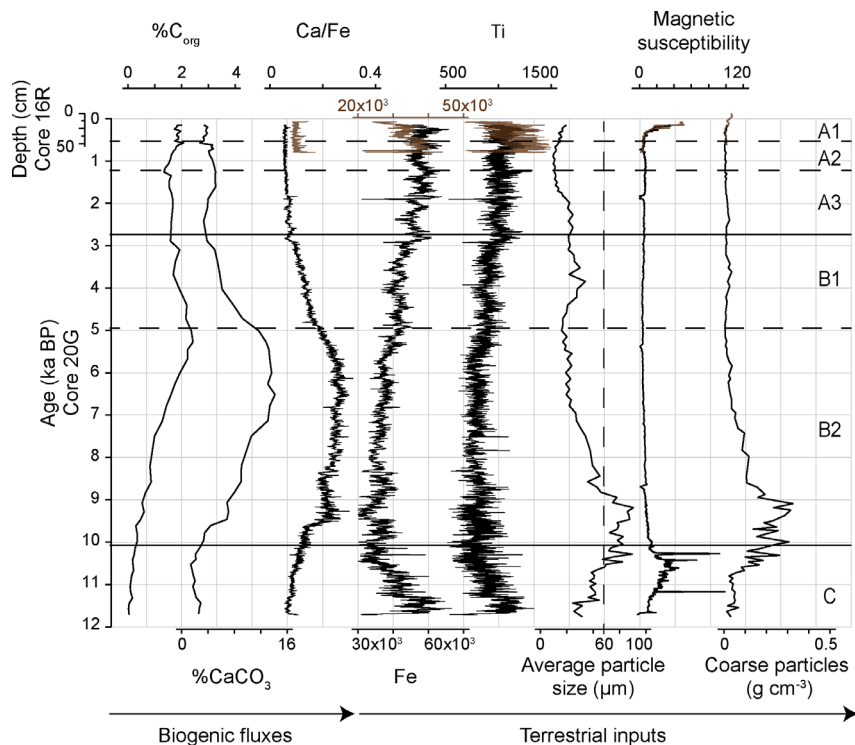


Fig. 3. Results of sedimentological and geochemical analyses of cores from station SA13-ST3 (20G in black and 16R in brown) and their physical properties: average particle size, magnetic susceptibility and weight of the coarse particles ( $<106 \mu\text{m}$ ) from the palynological preparations. Zones defined from the PCA are indicated to the right (see Fig. 4).

~2.4% at ~5 ka BP, after which it slightly decreases until ~1 ka BP although remaining >~1.6% (Fig. 3). The  $C_{\text{org}}/C_{\text{inorg}}$  ratio (cf. Fig. S1) reaches a maximum between about 3.8 and 1.8 ka BP, then after 0.7 ka BP. This suggests major changes in the nature of biogenic fluxes and/or preservation (biogenic carbonates vs. organic remains).

### Palynological assemblages

The palynological assemblages of cores 20G and 16R are dominated by dinocysts with concentrations ranging from  $1.1 \times 10^3$  to  $3.2 \times 10^5$  cysts  $\text{cm}^{-3}$ , which allows to calculate fluxes in the order of  $10^2$  to  $10^4$  cysts  $\text{cm}^{-2} \text{a}^{-1}$  (Fig. 4). The concentrations of organic linings of benthic foraminifers are  $2.7 \times 10^2$  to  $8.5 \times 10^4$   $\text{cm}^{-3}$  (fluxes from  $10^1$  to  $10^3$   $\text{cm}^{-2} \text{a}^{-1}$ ), those of *Halodinium* spp.  $4.7 \times 10^2$  to  $1.7 \times 10^4$   $\text{cm}^{-3}$  (fluxes from  $10^1$  to  $10^3$   $\text{cm}^{-2} \text{a}^{-1}$ ) and

maximum concentrations of pollen grains and spores are  $3.2 \times 10^3$   $\text{cm}^{-3}$  (fluxes  $10^2$   $\text{cm}^{-2} \text{a}^{-1}$ ) (Fig. 4, Table S5).

A total of 18 dinocyst taxa were identified: 16 taxa are common, occurring in more than five samples, and 14 represent more than 99% of the assemblages. The 10 dominant taxa are phototrophic dinoflagellate species. They include *Impagidinium pallidum*, *Nematosphaeropsis labyrinthus*, *Operculodinium centrocarpum*, *Spiniferites elongatus*, *Spiniferites ramosus* and *Pentaparsodinium dalei*. Heterotrophic taxa include *Islandinium minutum*, *Islandinium? cezare*, *Brigantedinium* spp. and *Selenopemphix quanta* (Fig. 4). Before ~10 ka BP, phototrophic taxa are rare but *Impagidinium pallidum*, *Nematosphaeropsis labyrinthus*, *Operculodinium centrocarpum*, *Spiniferites elongatus* and *Spiniferites ramosus* occur in low percentages. *Nematosphaeropsis labyrinthus* starts to increase around ~7 ka BP, with its maximum in the upper part of the core (<4 ka BP). *Operculodinium centrocarpum*

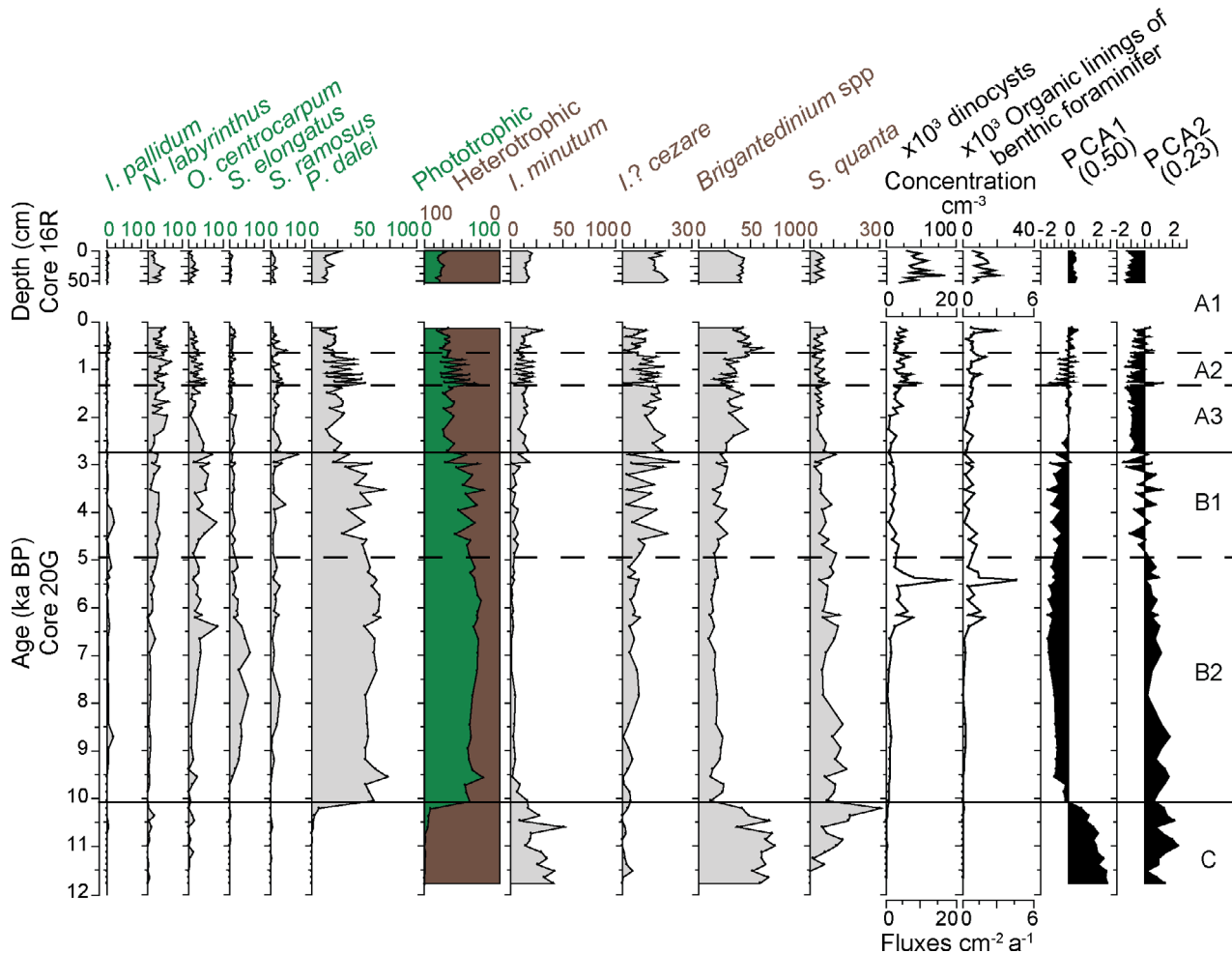


Fig. 4. Percentage of the dominant dinocyst taxa, concentrations, fluxes of the main palynomorphs and scores of axes 1 and 2 from the principal component analysis (PCA) of dinocyst assemblages. The two axes explain together 73.64% of the variance. The cumulative percentages of phototrophic and heterotrophic taxa are shown in green and brown, respectively. Based on PCA axes 1 and 2, we distinguished three zones (A, B, C) and five subzones A1, A2, A3 and B1, B2. The percentages of all dinocyst taxa are reported in Fig. S2.

records maximum percentages ranging between ~5 and ~2.5 ka BP and *Spiniferites elongatus* between ~9.5 and ~6 ka BP. The cyst of *Pentapharsodinium dalei* is dominant with up to 50% from ~10 to ~3 ka BP. The heterotrophic taxa dominate before 10 ka BP and after 3 ka BP. *Islandinium minutum* records a first maximum (~30%) before 10 ka BP and a second (~15%) after 3 ka BP. *Brigantedinium* spp. shows a similar distribution with up to 50% before 10 ka BP and about 40% during the last 3000 years. *Islandinium? cezare* progressively increases from an average of 1.5% before 10 ka BP to ~20% in the top of the sequence. *Selenopemphix quanta* is common all along the core with an average of 4–8% (Fig. 4).

The first axis (PCA 1) explains 50.41% of the variance. It is characterized by a positive correlation with *Islandinium minutum* and *Brigantedinium* spp. and by a negative correlation with the cysts of *Pentapharsodinium dalei* and other dominant taxa (Fig. 5A). The second axis (PCA 2) explains 23.23% of the variance and shows positive scores for *Selenopemphix quanta*, *Spiniferites elongatus*, and negative scores for *Islandinium? cezare*, *Nematosphaeropsis labyrinthus* and other taxa (Fig. 5A).

The PCA 1 scores are used to define three main zones labelled A, B and C (Fig. 4). The major change in assemblages at about 10 ka BP, from C to B (Figs 4, 5) corresponds to a shift from strongly positive to negative PCA 1 scores, which is marked by a significant increase of phototrophic taxa (Fig. 4). From zone B to zone A, there is a recurrence of dominant heterotrophic taxa (Figs 4, 6). The PCA 2 scores show a switch from positive to negative values at ~5 ka BP, which led us to split zone B into subzones B2 and B1, from ~10 to ~5 ka BP and from ~5 to ~2.7 ka BP, respectively (Fig. 4). Zone A, which is

defined based on negative scores of PCA 2 and PCA 1 close to zero, can be subdivided into three subzones: A3, from ~2.7 to ~1.3 ka BP with a PCA 1 close to zero, A2 from ~1.3 to ~0.65 ka BP with high frequency variation of positive to negative PCA 1 scores and finally, A1 from ~0.65 to 0 ka BP with slightly positive PCA 1 scores (Fig. 4).

#### Reconstruction of sea-surface parameters

Zone C (from ~12 to ~10 ka BP) is characterized by low species diversity and low fluxes (Fig. 4), which is typical of cold environments (de Vernal *et al.* 2020). The quantitative estimates indicate dense sea ice cover from 4 to 10 months per year, low summer SST ranging from 0 to 6 °C, low summer primary productivity (PP) ~800 mg C m<sup>-2</sup> d<sup>-1</sup> and summer SSS ~33 psu (Fig. 6).

Subzone B2 (from ~10 to ~5 ka BP) is marked by high summer PP of ~2.9×10<sup>3</sup> mg C m<sup>-2</sup> d<sup>-1</sup>, high summer SST ranging from 6 to 12 °C with an average of ~9 °C and low summer SSS of ~30 psu (Fig. 6). After ~5 ka BP, subzone B1, spanning from ~5 to ~2.7 ka BP, records an increased variability of the sea-surface conditions, along with an increase of summer SSS to ~31 psu and a decrease of summer SST to ~8 °C and summer PP ~2×10<sup>3</sup> mg C m<sup>-2</sup> d<sup>-1</sup>.

Subzone A3 (from ~2.7 to ~1.3 ka BP) is characterized by cold conditions with summer SST of ~5 °C, low summer PP of ~1.4×10<sup>3</sup> mg C m<sup>-2</sup> d<sup>-1</sup> and summer SSS of ~32 psu (Fig. 6). Subzone A2 (from ~1.3 to ~0.65 ka BP) and subzone A1 (after ~0.65 ka BP) are marked by high instability, with large amplitude oscillation of summer SST, from ~3 to ~12 °C, salinity, from ~29 to ~33 psu, and productivity (PP), from ~7.1×10<sup>2</sup> to

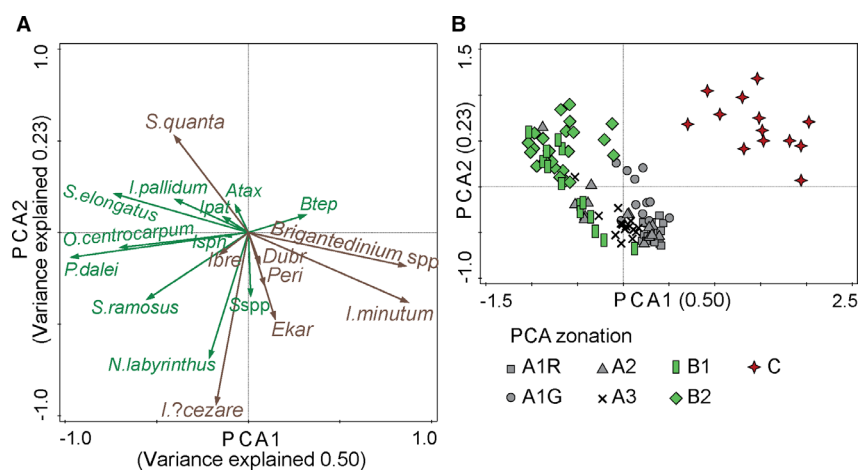


Fig. 5. A. Ordination diagram of the dinocyst taxa from down-core assemblages according to PCA 1 and PCA 2. The taxa plotted in the PCA are indicated either by their species name (dominant taxa) or by four-letter abbreviations (Atax = *Ataxodinium choane*; Btep = *Bitectatodinium tepikiense*; Ipat = *Impagidinium patulum*; Isph = *Impagidinium sphaericum*; Spss = *Spiniferites* spp.; Ibre = *Islandinium brevispinosum*; Ekar = *Echinidinium karaense*; Dubr = *Dubridinium* spp.; Peri = protoperidinioids). The phototrophic taxa are indicated in green and the heterotrophic taxa in brown. B. Ordination diagram of samples according to the assemblage zones as shown in Fig. 4.

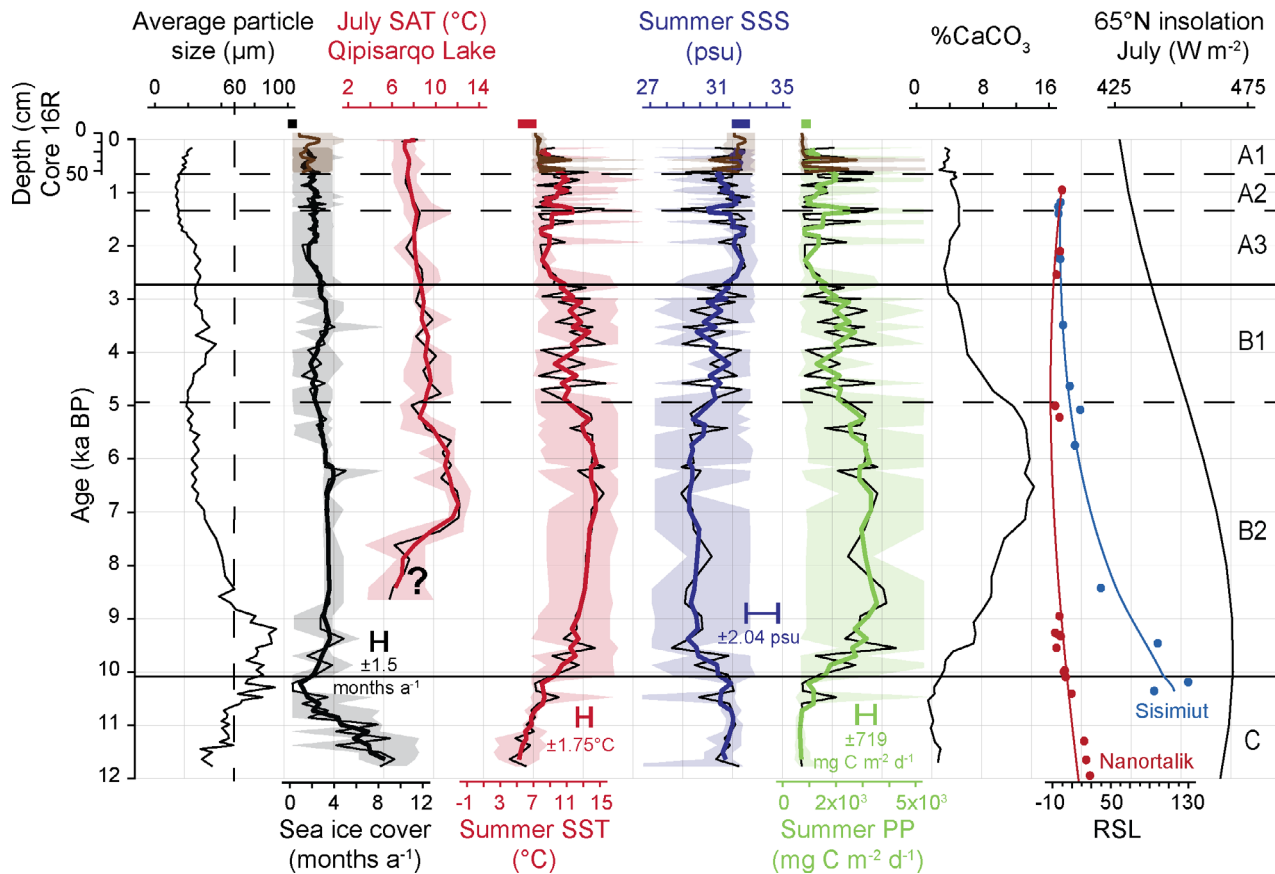


Fig. 6. Cores SA13-ST3: average particle size of the sediment, MAT reconstruction of sea ice cover concentration, summer sea-surface salinity (SSS), summer sea-surface temperature (SST), and summer primary productivity (PP) from dinocyst assemblages in cores SA13-ST3 (20G in colour and 16R in brown, the thick line shows a three-point running average) and calcium carbonate ( $\text{CaCO}_3$ ) content of the sediment. MAT reconstructions of July surface air temperature (SAT) from pollen grain assemblages at Qipisarqo Lake, southwest Greenland, are from Fr chet te & de Vernal (2009); the question mark indicates the uncertainties in the reconstructed SAT from pollen in the Early Holocene due to possible bias linked to early vegetation growth on rock surfaces eroded by ice. The relative sea level (RSL) curve was established from dates of shoreline elevations at Sisimiut (central West Greenland; Long *et al.* 2009; Bennike *et al.* 2011) and Nanortalik (South Greenland; Sparrenbom *et al.* 2006). The insolation at  $65^\circ\text{N}$  in July is from Berger & Loutre (1991). Instrumental values of present-day sea-surface conditions (National Snow and Ice Data Center; World Ocean Atlas 2013; MODIS R2018) are indicated by horizontal rectangles at the top of the sea-surface reconstructions and the shaded area around the reconstructions encompasses the minimum and maximum values according to the sets of five analogues. The error of prediction indicated by the horizontal bars applies to the most probable estimate calculated from the weighted average of the five best analogues (see Material and methods). Zones defined from the PCA are indicated to the right.

$\sim 3.6 \times 10^3 \text{ mg C m}^{-2} \text{ d}^{-1}$ . Moreover, a general cooling is recorded after 2.7 ka BP (Fig. 6).

Subzone A1 described from the gravity core is also recovered in the Rumohr lot core. The reconstructions of the sea-surface parameters from both cores are similar. At the top of the core, the last century recorded a return to relatively stable conditions with low SST, high SSS, low PP and absence of sea ice cover. The reconstructions at the top of the core fit within the range of modern instrumental data (Fig. 6).

In general, the reconstructions illustrate parallel fluctuations of summer SST and PP, which are opposite to salinity. As the values are from a modern database, which includes different combinations of these parameters, the similarity between the reconstructed variables is probably not an artifact of the methodological

approach. However, as the reconstructed values are made up of an interpolation of the best estimate from five analogues, the values may have resulted in smoothing of the records, but this should not change the overall picture.

#### Isotopic ( $^{18}\text{O}$ and $^{13}\text{C}$ ) data from benthic foraminifers

Among benthic foraminifers, *N. labradorica* is often used as an indicator of high productivity in sub-arctic settings (e.g. Bilodeau *et al.* 1994; Korsun & Hald 2000; Perner *et al.* 2011; Seidenkrantz *et al.* 2013a; Moros *et al.* 2016). It is common in the study core and permitted us to develop an almost continuous benthic isotopic record spanning from about 10.4 to 1 ka BP. No foraminifers were found in the core below 480 cm ( $>10.4$  ka BP), or in

the upper 70 cm of the sequence (<0.8 ka BP), for isotopic measurements.

*N. labradorica* recorded  $\delta^{18}\text{O}$  ranging from  $\sim 3.95$  to  $\sim 3.35\text{‰}$ , with a general decrease from  $\sim 10.4$  to  $\sim 6.7$  ka BP. The shift in  $\delta^{18}\text{O}$  from the Early to Middle Holocene may suggest a change in the properties of the shelf water, a warming of the bottom waters and/or a freshening and a decrease in salinity (Fig. 6) due to meltwater. After  $\sim 6.5$  ka BP, the  $\delta^{18}\text{O}$  of *N. labradorica* averages  $\sim 3.44\text{‰}$  (Fig. 7). The  $\delta^{18}\text{O}$  of *N. labradorica* varies within a range compatible with that of *N. labradorica* in a Disko Bay sediment core (Fig. 7; MSM343300, Ouellet-Bernier et al. 2014), but records a lower variability than the Disko Bay site, which is more closely influenced by meltwater from marine terminating glaciers and local ice streams. A large offset in *N. labradorica*  $\delta^{13}\text{C}$  values is observed between the Nuuk (Fig. 7; SA13-ST3-20G) and Disko Bugt (Fig. 7; MSM343300) cores during a relatively long interval of the Middle to Late Holocene transition ( $\sim 4.5$  until  $\sim 2$  ka). Strongly  $^{13}\text{C}$ -depleted values ( $-4.5 < \delta^{13}\text{C} < -3\text{‰}$ ) in the Nuuk core contrast with the relatively stable values of the Disko Bay record ( $\delta^{13}\text{C} \geq -2\text{‰}$ ) during this interval.

In the sediment core SA13-ST13-20G, the  $\delta^{13}\text{C}$  in organic matter ( $\delta^{13}\text{C}_{\text{org}}$ ) ranges from  $-22.8$  to  $-20.8\text{‰}$ . From 12 to 9.5 ka BP, the  $\delta^{13}\text{C}_{\text{org}}$  recorded two peaks of relatively high values ( $22.5$  to  $-21.4\text{‰}$ ). After 9.5 ka BP, the  $\delta^{13}\text{C}_{\text{org}}$  are characterized by a slight increase from  $-22.2$  to  $-21.6\text{‰}$ , with a shift between 2 and 1.3 ka BP toward values of  $-20.9\text{‰}$  (Fig. 7). Since marine and terrestrial organic matter are characterized by  $\delta^{13}\text{C}_{\text{org}}$

signatures around  $-20$  to  $-22\text{‰}$  and  $\sim -27\text{‰}$ , respectively (Meyers 1994, 1997; Muzuka & Hillaire-Marcel 1999), the  $\delta^{13}\text{C}_{\text{org}}$  values in core SA13-ST13-20G indicate organic matter from a predominantly marine source. The isotopic composition in the lower part of the core corresponding to the Early Holocene, however, suggests slightly more pronounced terrestrial inputs. The isotope data ( $\delta^{13}\text{C}_{\text{org}} > -22\text{‰}$ ) in the upper part of the core encompassing the Common Era, in contrast, suggest particularly high fluxes of marine organic carbon.

## Discussion

### *Palynomorph preservation and source of organic matter*

Despite some changes in mean grain size, particularly prior to  $\sim 9$  ka BP, with significant ice-rafting deposition indicated by the sand content (Figs 3, 6, 7), the sediment grain size, mostly silty-clay, varies little aside from large-wavelength minor-amplitude oscillations in response to biogenic carbonate accumulation rate (Fig. 3). Additionally, as the semi-quantitative abundance of Fe follows quite closely that of Ti (Fig. 3), some gradual changes in detrital supplies after  $\sim 9$  ka BP are notable, but do not show significant diagenetic chemical evolution of the iron content. Finally, although dinoflagellate cysts are extremely resistant to degradation (e.g. Dale 1996), the cysts of some heterotrophic taxa such as *Brigantedinium* are sensitive to oxidation (e.g. Zonneveld et al. 2001, 2008). In our study, organic matter is abundant (Fig. 3) and *Brigantedinium* is common to

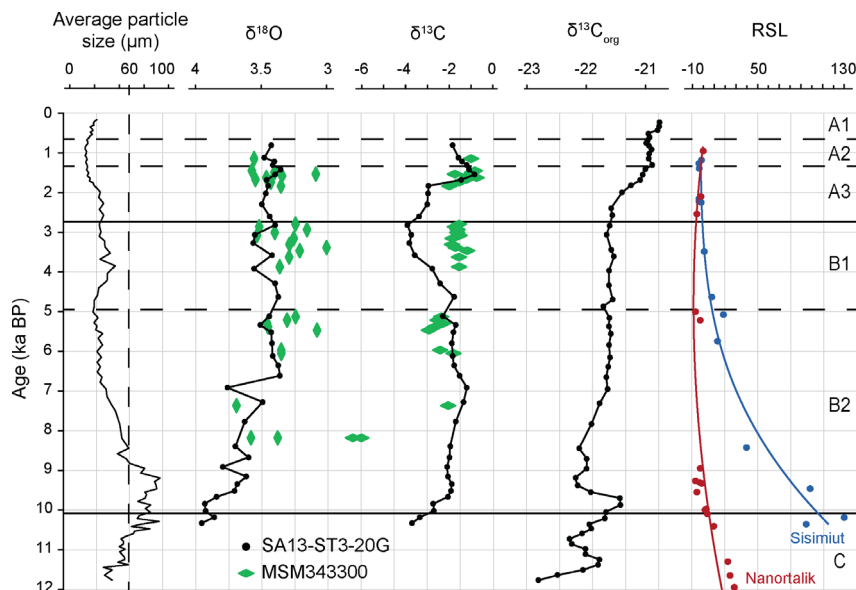


Fig. 7. Average particle size of the sediment core SA13-ST3-20G. Isotopic compositions,  $\delta^{18}\text{O}$  and  $\delta^{13}\text{C}$  (‰ vs. VPDB) of *Nonionellina labradorica* tests from the core SA13-ST3-20G (dots) and MSM343300 (diamonds; Ouellet-Bernier et al. 2014). In core MSM343300, *N. labradorica* tests were picked up in the sediment fractions  $>250 \mu\text{m}$ , whereas specimens from  $>100 \mu\text{m}$  were used for the setting of the isotopic curve of SA13-ST3-20G. Carbon isotopic signature,  $\delta^{13}\text{C}_{\text{org}}$  (‰ vs. VPDB), of the sediment from the core SA13-ST3-20G. Relative sea level (RSL) as in Fig. 6. Zones defined from the PCA are indicated to the right.

abundant (Fig. 4) with the cysts showing no sign of degradation throughout the sequence (Fig. 4). Together, these indications suggest a relatively uniform sedimentary regime at the study site and excellent preservation conditions, at least during the Middle and Late Holocene.

The  $\delta^{13}\text{C}_{\text{org}}$  suggests predominant input from marine productivity throughout the study sequence, with perhaps some terrestrial inputs during the Early Holocene. Hence, the overall data seem to indicate mostly pelagic fluxes and very good preservation of the organic material, with the exception of some intervals of the Early Holocene, during which coarser grain size and slightly lower  $\delta^{13}\text{C}_{\text{org}}$  may indicate episodes marked by detrital inputs, possibly related to regional ice retreat as indicated from relative sea-level changes in the Sisimiut area (Figs 6, 7). However, significant changes in currents can be excluded for from the Middle to the Late Holocene, as illustrated by the relatively steady current-sensitive parameters, in particular grain size vs.  $\text{CaCO}_3$  and magnetic susceptibility (Fig. 3). In addition, most studies documenting the distribution of dinocysts on the sea floor indicate regionalism of assemblages and limited impact of distal inputs. Analyses of surface sediments from the southwest Greenland margin show strong gradients in the dinocyst taxa distribution (Allan *et al.* 2020), suggesting clear boundaries linked to proximal fluxes.

#### Palynological content

Heterotrophic dinoflagellates may survive in the dark Arctic ecosystem and their abundance in sediment is often related to diatom production (e.g. Radi & de Vernal 2008; Heikkilä *et al.* 2014, 2016; de Vernal *et al.* 2020). The quasi-exclusive dominance of heterotrophic taxa and the extremely low concentrations of dinocysts in the bottom of the core together illustrate harsh conditions and at least as long seasonal sea ice cover (Figs 4, 5B, 6). The rapid increase in species diversity and dinocyst concentrations, and the high abundance of phototrophic taxa from 10 ka BP towards the present (Fig. 4) likely relate to an increase of productivity and light availability. The cysts of *Pentaparsodinium dalei* are often found in stratified waters and may be linked to low salinity related to freshwater meltwater input together with primary productivity (Rochon *et al.* 1999; Heikkilä *et al.* 2014; Allan *et al.* 2020). Its dominance, from 10 to 3 ka BP (Fig. 4), could be related to the late summer bloom due to meltwater input (e.g. Boertmann *et al.* 2013; Juul-Pedersen *et al.* 2015; Allan *et al.* 2020), while its subsequent decline, relative to heterotrophic taxa such as *Islandinium minutum*, *Islandinium? cezare* and *Brigantedinium* spp. (Fig. 4), suggests the recurrence of cold conditions (Allan *et al.* 2020) during the Neoglacial.

#### The regional deglaciation and Fiskebanke moraines

The Fiskebanke moraines, located on the inner shelf of southwest Greenland in front of the Sukkertoppen ice cap area, have been suggested to date from the Younger Dryas (Funder *et al.* 2011; Cofaigh *et al.* 2013), whereas the Outer Hellefisk moraines have been suggested to date to Marine Oxygen Isotope Stage 4 (MIS 4; 71–57 cal. ka BP; Seidenkrantz *et al.* 2019). In the Godthåbsfjord system, the retreat of the GrIS from the coastline to inland occurred between ~11.4 and ~10.4 ka BP, with a rate of about  $125 \text{ m a}^{-1}$ , although the mouth of the Godthåbsfjord was deglaciated late at ~10.7 ka BP (cf. Larsen *et al.* 2014; Larsen *et al.* 2017). The oldest  $^{14}\text{C}$  date from the core 20G is at a depth of 514 cm and yields a mean age of ~10.7 ka BP (Fig. 2; Table 1). Due to the lack of datable material, it was not possible to develop a precise chronology in older sediments, which makes the lowest 73 cm difficult to discuss. Nevertheless, the sediments from the bottom of the core consist of relatively coarse-grained material with high magnetic susceptibility and an elemental composition with high proportions of Fe and Ti indicating dominant terrestrial input (Fig. 3). Together with extensive sea ice cover, inferred from the dinocyst assemblages characterized by quasi-exclusive dominance of heterotrophic taxa and the low dinocyst abundance (Figs 4, 5B, 6), the elemental composition suggests rapid sediment accumulation in an ice-proximal environment. Adding to these observations, the chronology of the end moraines in southwestern Greenland (cf. Briner *et al.* 2020) and the rapid sea-level change of the Early Holocene (Long *et al.* 2011), we can assess that the GrIS margin was located close to our study site and sediment deposition consequently corresponding to the bottom of core SA13-ST3-20G. This would explain the reconstructed harsh conditions, although they could also be related to a cold late Younger Dryas climate (YD; end ~11.7 cal. ka BP; Alley *et al.* 2010; Jennings *et al.* 2014), in agreement with the proposed age of the Fiskebanke moraines (Funder *et al.* 2011; Cofaigh *et al.* 2013). Shortly following ~10.7 ka BP, an increase in sand-sized particles and magnetic susceptibility may indicate a rapid retreat of the ice margin accompanied with ice calving and IRD, at the same time as the slight increase of phototrophic taxa and reconstructed decrease in sea ice cover (Figs 3, 4, 6).

#### Hydrographic conditions during the Holocene

The combined records of dinocyst assemblages, benthic foraminiferal isotopes and sedimentological data permit inferences about both surface and bottom water conditions at the study site (Figs 3, 4, 6, 7). As mentioned above, the decreasing  $\delta^{18}\text{O}$  values of *N. labradorica*, from the base of the sequence to the ~7 ka BP-dated layer, may record either a decreasing salinity or a warmer water

mass. Combining a large array of proxies, Ouellet-Bernier *et al.* (2014) concluded that a progressive penetration of a ‘warmer’ WGC along the western Greenland margin occurred during this transition. The responses of  $\delta^{18}\text{O}$  values of *N. labradorica* at Disko Bay and off Nuuk, as well as the increasing summer temperatures offshore and inland (Fig. 6), lead us to conclude that this Early to Middle Holocene interval led to the inception of a warmer WGC by  $\sim 7$  ka BP (Figs 3, 4, 7). This warming is related to the development of the Irminger current in the NW North Atlantic (Ólafsdóttir *et al.* 2010). Whereas benthic foraminiferal studies suggested that Atlantic waters were likely flowing as a subsurface current on the shelf off Ummannaq, West Greenland, and in the Nares Strait in northern Baffin Bay as early as  $\sim 14$  ka BP (Knudsen *et al.* 2008; Sheldon *et al.* 2016; Jennings *et al.* 2017), the warming of the subsurface waters of the WGC is recorded at about  $\sim 7.7$  ka BP along the northwest Greenland margins in the Baffin Bay (Levac *et al.* 2001; Caron *et al.* 2019), and at about  $\sim 7.3$  ka BP in the inner Disko Bay, north of the Davis Strait (core MSM343300; Ouellet-Bernier *et al.* 2014). At our study site south of Davis Strait, the postglacial warming of surface waters, associated with an increased inflow of Atlantic waters through the WGC, is dated at  $\sim 7$  ka BP, in phase with the minimum benthic  $\delta^{18}\text{O}$  value of  $\sim 3.5\text{‰}$  (Fig. 7). Such timing is consistent with the onset of intermediate-deep water formation in the Labrador Sea (Hillaire-Marcel *et al.* 2001; Gibb *et al.* 2015) and would correspond to an important regional benchmark. Optimal thermal conditions in surface waters persisted until about 5 ka BP. On land, at the Qipisarqo Lake in southern Greenland, the July surface air temperature (SAT) estimated from pollen grains was  $\sim 10$  to  $\sim 12$  °C from  $\sim 7.5$  to  $\sim 5.5$  ka BP (Fréchette & de Vernal 2009). Off Nuuk as well as onshore in southern Greenland, the HTM seems to have been regionally consistent, and furthermore appeared to have been in phase with the GrIS retreat (Briner *et al.* 2016). In general, the climate of western and central Greenland was warmer by about 2 °C during the Middle Holocene (Kobashi *et al.* 2017). Such warm conditions leading to enhanced meltwater discharge could be at the origin of particularly strong stratification of the upper water layer (Fig. 6).

Progressive cooling of the surface waters at site SA13-ST3 took place after  $\sim 5$  ka BP. At Qipisarqo Lake, July SAT indicated a cooling of 1–2 °C after  $\sim 5.5$  ka BP (Fig. 6; Fréchette & de Vernal 2009). Off Nuuk, our data show decreased SST, but also high-amplitude variations with pronounced cooling pulses between  $\sim 5$  and  $\sim 4$  ka BP as depicted from variable proportions of *Islandinium? cezare* and the cysts of *Pentapharsodinium dalei* (Figs 4, 6). The variability of sea-surface conditions tends to suggest a non-monotonic cooling and an oscillatory mode linked with the respective strength of the North Atlantic currents contributing to the WGC and cold flow

from the EGC or proximal meltwater supply. From  $\sim 4$  to  $\sim 2.7$  ka BP, the dinocyst data suggest relatively low SSS and high SST (Figs 4, 6). After  $\sim 2.7$  ka BP, the increase of heterotrophic taxa, such as *Islandinium minutum*, *Islandinium? cezare* and *Brigantedinium* spp. (Fig. 4), suggests the recurrence of cold conditions (Allan *et al.* 2020), which probably led to generally low summer SST and high SSS, similar to the present-day (Fig. 6). Variations in percentages of the cysts of *Pentapharsodinium dalei* and the reconstruction of sea-surface conditions also suggest warming phases from  $\sim 1.6$  to  $\sim 1.25$  ka BP and from  $\sim 1.1$  to  $\sim 0.6$  ka BP (Figs 4, 6, 8). The warming around  $\sim 1.5$  ka BP coincided with increased estimated PP and  $\delta^{13}\text{C}$  in benthic foraminifers, suggesting a major oceanographic change (Figs 4, 7). These episodes of relatively warm conditions seem to correspond to regional features recorded both in the surface and sub-surface water layers (see Fig. 8). In Ameralik fjord, from  $\sim 1.6$  to  $\sim 1.2$  ka BP, the benthic foraminiferal assemblages reflect increased advection of warm and saline Atlantic waters (Seidenkrantz *et al.*

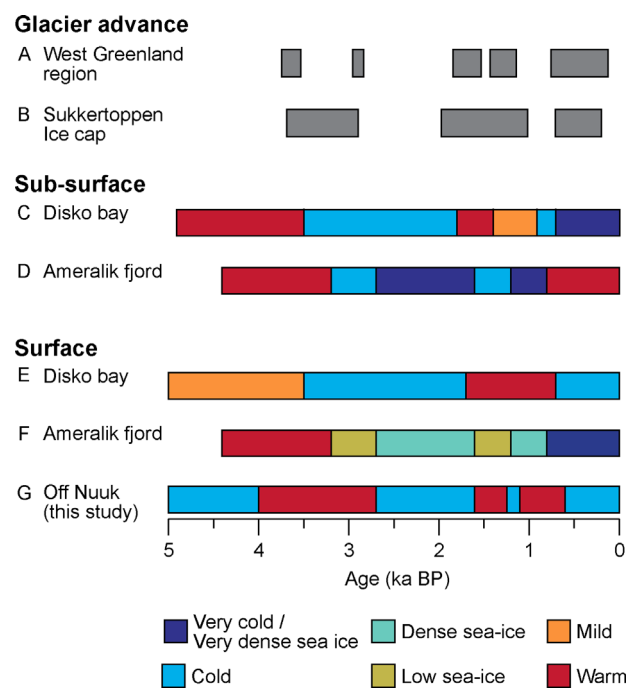


Fig. 8. Transition from warm to cold conditions along the West Greenland margin. A. Timing of local glacier advances in West Greenland region (Larsen *et al.* 2017; Levy *et al.* 2017; Schweinsberg *et al.* 2017). B. Timing of the local glacier regrowth in Sukkertoppen ice cap area (Schweinsberg *et al.* 2018). C. WGC properties at the sub-surface as deduced from benthic foraminiferal assemblages in the Disko Bugt (Perner *et al.* 2013; Moros *et al.* 2016). D. Strength of WGC advection in the Ameralik fjord based on benthic foraminiferal assemblages (Seidenkrantz *et al.* 2007). E. Summary of sea-surface conditions in Disko bay based on multiproxy data (Moros *et al.* 2016). F. Sea ice cover based on diatoms assemblages in the Ameralik fjord (Seidenkrantz *et al.* 2007). G. Summary of sea-surface conditions at the study site based on dinocyst assemblages (this study; cf. Fig. 5). Site location shown in Fig. 1.

2007); at Disko Bay, a warming was also identified from ~1.8 to ~0.9 ka BP in the bottom water (Perner *et al.* 2013). Hence, even though the precise timing of changes recorded in the different cores is not exactly the same, which is possibly due to uncertainties in the chronology, the overall data suggest variations in the strength of the North Atlantic water contribution to the WGC that are roughly consistent over the southwest Greenland margins, at least since ~5 ka BP (Fig. 8).

Finally, our data indicate a cooling in surface and sub-surface waters after ~0.6 ka BP (Figs 5B, 6; Zone A1). It seems to correspond to the regional onset of the Little Ice Age (LIA) in western Greenland, where decreasing surface air temperature and local glacier regrowth were recorded at about the same time (Fig. 8; Funder *et al.* 2011; Young & Briner 2015; Briner *et al.* 2016; Larsen *et al.* 2017; Schweinsberg *et al.* 2018). Off Nuuk, the LIA is characterized by a decrease in summer SST and PP and an increase of SSS, which probably relate to a decrease in meltwater discharge. It is also marked by increased magnetic susceptibility, Ti and Fe content, which together reflect detrital input with values almost as high as those during deglaciation, thus suggesting input from glacial erosion (Figs 3, 6).

#### *Ocean–ice-sheet relationship*

In the Godthåbsfjord system, the GrIS experienced rapid retreat toward its present margin between ~11.4 and ~10.4 ka BP (Larsen *et al.* 2014, 2017), and thereafter the glacier seemed to continue to retreat until ~7.7–7.5 ka BP (Seidenkrantz *et al.* 2013a). The synthesis of the GrIS ice mass balance by Larsen *et al.* (2015), which focussed on southern Greenland, indicated that maximum ice retreat occurred from ~8 to ~5 ka BP with a centennial ice loss rate as high as 100 Gt a<sup>-1</sup> for several millennia in this interval. The synthesis of Holocene temperature reconstructions from Arctic Canada and Greenland by Briner *et al.* (2016) pointed to a warm period between ~9 and ~5 ka BP. Moreover, the synthesis of the southwest GrIS retreat from Lesnek *et al.* (2020) documented a maximum of retreat between ~10.4 and 9.1 ka, and retreat rates decreasing after ~7.3 ka. In our study, the thermal maximum seems to correspond to the dominance of phototrophic taxa (Fig. 4) that led us to reconstruct maximum summer SST, PP and minimum SSS from ~9.5 to ~5 ka BP (Fig. 6). We interpret the contrast between SST and SSS as the consequence of GrIS meltwater discharge under warm climate, thus resulting in a dilution of surface water and low surface-water salinities (cf. also Gibb *et al.* 2015). Relatively fresh surface water in the Labrador Sea during the Early Holocene has been documented from several studies (Hillaire-Marcel *et al.* 2001; Solignac *et al.* 2004; de Vernal & Hillaire-Marcel 2006; Gibb *et al.* 2015; Hoogakker *et al.* 2015), indicating that a basin-wide stratification delayed the formation of the modern deep water in the Labrador Sea until about

7 ka BP (Hillaire-Marcel *et al.* 2001; Hoogakker *et al.* 2015).

In the Sukkertoppen region, north of Maniitsoq (Fig. 1), the mountain glaciers experienced net recession until ~4.6 ka BP, followed by subsequent net regrowth (Schweinsberg *et al.* 2018). Major GrIS and local glacier expansions were recorded at ~3.6–3.5 ka BP in southwest Greenland (Larsen *et al.* 2017; Schweinsberg *et al.* 2017, 2018). They were associated with a decrease in summer air temperatures of about 1 to 2 °C (Larsen *et al.* 2017). Many local glacier advances in west Greenland, notably at ~3.7–3.6, ~2.9, ~1.8–1.7, ~1.7–1.6, ~1.4–1.2, ~0.8–0.7 and ~0.5 ka BP, were also recorded (Larsen *et al.* 2017; Levy *et al.* 2017; Schweinsberg *et al.* 2017, 2018; see Fig. 8). The multiple phases of ice expansion point to a centennial-scale variability superimposed on longer-term changes forced by decreasing summer solar insolation. At our study site, we also reconstructed high frequency variations in SST and SSS, suggesting that instabilities characterized the surface waters off southwest Greenland. It is noteworthy that summer SST and SSS estimates fluctuate in opposition, with variations corresponding to shifts from low salinity-high temperature sea-surface conditions to high salinity-low temperature. Such opposite variations are not a methodological artifact since estimates are based on modern analogues without calibration. They rather illustrate oscillations along a gradient from estuarine to oceanic conditions. Hence, our record probably suggests changes in surface water stratification and thermal inertia, with higher surface salinity and lower temperature corresponding to lesser stratification, possibly linked to episodic flow of the WGC at the surface. Conversely, lower surface salinity and higher temperature would reflect freshwater discharges, shoaling of the surface layer and less thermal inertia fostering summer warming. However, very high temporal resolution with precise timing would be necessary to infer linkages between the local glacier dynamics and surface ocean conditions.

#### *Meltwater discharge and marine primary productivity*

In Arctic and sub-arctic seas, primary productivity is controlled directly by light and nutrient availability, which indirectly depend upon meltwater discharge, vertical mixing of the water column and sea-ice extent (Juul-Pedersen *et al.* 2015; Tremblay *et al.* 2015). The spring bloom is triggered by the increase of solar irradiance, together with the stabilization of the water column (Boertmann *et al.* 2013). In summer and autumn, continued primary production has been observed in glacial fjords in southwest Greenland. One of the driving forces in fjords with marine-terminating glaciers is basal meltwater discharge from these glaciers, which contributes to upwelling of nutrients from deeper waters into the photic zone (Boertmann *et al.* 2013; Juul-Pedersen

et al. 2015; Meire et al. 2017). Recent studies from the Godthåbsfjord and Fyllas Banke have shown a planktonic productivity succession with blooming of diatoms and haptophytes in spring, followed by diatoms in summer and by dinoflagellates and ciliates through summer, autumn and winter (Krawczyk et al. 2015, 2018).

In southwest Greenland, the maximum GrIS recession occurred between ~10.4 and 9.1 ka (Lesnek et al. 2020). In the GISP2 ice-core, the highest melt-layer frequency is recorded from 8.5 to 5.5 ka BP (Alley & Anandakrishnan 1995; Briner et al. 2016). Hence, we may infer that the low sea-surface salinity we reconstructed here from ~9 to ~5 ka BP (Fig. 6) is related to the meltwaters from the GrIS margins. Furthermore, from ~10 to ~5 ka BP, the estimated summer PP is very high, up to  $\sim 3 \times 10^3 \text{ mg C m}^{-2} \text{ d}^{-1}$ . From ~10 to ~5 ka BP, the  $\delta^{13}\text{C}$  of *N. labradorica* is also characterized by high values ( $> -2.50\text{‰}$ ), which may suggest high marine PP (Figs 6, 7), likely associated with biogenic calcium carbonate fluxes as reflected by the relatively high  $\text{CaCO}_3$  and  $\text{C}_{\text{org}}$  concentrations and Ca/Fe ratio (Fig. 3). Consequently, we may hypothesize that the enhanced melting of tidewater glaciers in the Godthåbsfjord area was favourable for high nutrient inputs through upwelling until about 5 ka BP. This follows a major change in the productivity as demonstrated by the sharp changes in the proportion of organic vs. inorganic carbon, relative increase in  $\text{C}_{\text{org}}$  vs.  $\text{C}_{\text{inorg}}$  (Fig. S1), and a decrease of  $\delta^{13}\text{C}$  in *N. labradorica* shells (Figs 3, 7), driven by a decrease in biogenic carbonate fluxes, possibly related to a decrease in primary productivity (Fig. 6). It seems to be a local feature, as it is not recorded to the north in the Disko Bay (Fig. 7). Therefore, we associate the major change in productivity and carbon fluxes at site SA13-ST3 off Nuuk with the retreat of the ice margin in southern Greenland. Since 12 ka BP, the relative sea level dropped by at least 20 m in the area of Nanortalik to more than 100 m in the area of Sisimiut to reach close to present sea level by 4 ka BP (Long et al. 2011; Figs 6, 7). It is possible that a relatively high sea level contributed to an enhanced primary productivity during the Middle Holocene as higher sea levels would increase the presence of marine-terminating glaciers despite the retreating of the glaciers inland, which would have favoured a deeper upwelling.

#### Climate changes related to human history

The history of human settlement in West Greenland is characterized by the arrival and disappearance of several cultures over the past 4500 years (Jensen 2006; D'Andrea et al. 2011). It has been suggested that climate and environmental change was the major cause for this pattern (McGovern 1991; McGhee 1996; Jensen 2006; D'Andrea et al. 2011). The results from site SA13-ST3 permit us to propose a relationship between the surface ocean conditions and the human colonization phases

(Fig. 9). The arrival of the Saqqaq people corresponds to a warm period with a high summer SST and PP (Fig. 9). As the Saqqaq were open water hunters (Jensen 2006; D'Andrea et al. 2011), such climatic conditions were probably suitable for their livelihood. At ~2.7 ka BP, the cooling over western Greenland that led to glacier expansion together with the decrease in marine PP (Fig. 9) may have made subsistence more difficult for the Saqqaq culture, which was replaced by the Dorset people, who specialized in sea-ice hunting (Jensen 2006; D'Andrea et al. 2011). At ~2 ka BP, the changes towards unstable conditions seem to coincide with the gap of about 1000 years in human occupation in western Greenland. By ~1 ka BP, relatively warm conditions and PP increase correspond to the arrival of the Norse, who were a sedentary people who initially relied on livestock (Fig. 9). Finally, at the beginning of the LIA, about 650 years ago, a strong climate deterioration accompanied by glacial advance might have contributed to the demise of the western Norse settlements (D'Andrea et al. 2011), leaving the area to the Thule people, ancestors of the modern Greenlandic Inuit, who arrived in Greenland 850 years ago (McGovern 1991). Our study suggests that not only climate conditions, but also marine productivity may have played an important role in the human occupations along the southwest Greenland coasts (Fig. 9).

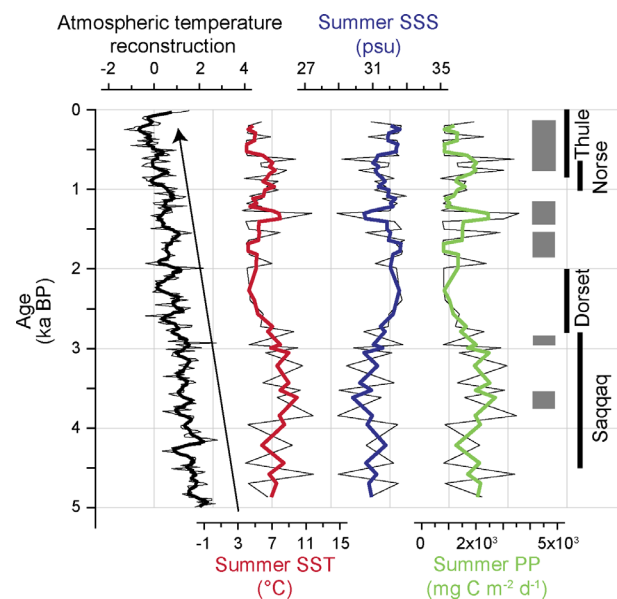


Fig. 9. Greenland temperature reconstruction from Vinther et al. (2009) using proxy data from six ice-cores; the arrow indicates the Neoglacial cooling. Dinocyst-based reconstruction of summer sea-surface temperature (SST), salinity (SSS), and primary productivity (PP) in core SA13-ST3 (this study; the thick line shows a three-point running average). The grey rectangles indicate local glacier advances in West Greenland region (Larsen et al. 2017; Levy et al. 2017; Schweinsberg et al. 2017, 2018). On the right, the main phases of human occupation in West Greenland after d'Andrea et al. (2011).

## Conclusions

Investigation of the sediment cores SA13-ST3-20G and SA13-ST3-16R located on the West Greenland shelf just north of Nuuk allowed us to document variations in sea-surface and bottom water conditions, and to propose relationships with the dynamics of the southern GrIS and mountain glaciers throughout the Holocene.

Our record illustrates that the central West Greenland shelf was characterized by extensive sea ice cover, high terrestrial inputs and rapid sedimentation, likely related to a nearby ice shelf margin, potentially linked to the Fiskebanke moraines, until about ~10.7 ka BP. At that time, rapid deglaciation occurred, accompanied by increasing summer surface water warming, with sea surface temperatures reaching up to ~10 °C. During the Early Holocene, the retreating GrIS led to elevated meltwater discharge along the shelf and upwelling. We record cooling starting at ~5 ka BP, with an increase in the variability of surface waters and cold pulses marked by harsh conditions that possibly coincide with phases of glacier expansions.

This work highlights the close interaction between the changes in ocean water masses and ice-margin history of the GrIS and glaciers during the Holocene. We suggest that a combination of hydrographic conditions, regional climate and marine productivity influenced human cultural migration and development related to the Saqqaq, Dorset, Norse and Thule cultures.

*Acknowledgements.* – The authors are grateful to the captain, crew and scientific party of the RV ‘Sanna’, for retrieval of the sediment cores and CTD measurements. Thanks are due to Charlotte Rasmussen who assisted with the grain-size analyses. We are also grateful for the work of Bassam Ghaleb, Geotop-UQAM, who carried out the <sup>210</sup>Pb analyses, to Jean-François Hélie for his help with stable isotope analyses and to Anne Thøisen at the Department of Geoscience and Natural Resources, University of Copenhagen, who carried out the calcium carbonate analyses. We would also like to thank Dr Antoon Kuijpers, Geological Survey of Denmark and Greenland, for valuable discussion regarding the Fiskebanke moraines. The RV ‘Sanna’ expedition was funded by the Arctic Research Centre, Aarhus University, while the subsequent research was funded through grants from the Natural Science and Engineering Research Council (NSERC) of Canada and the *Fonds pour la Recherche du Québec Nature et Technologie* (FRQNT), the National Science Foundation (NSF, grant ARC-1504267), and the Independent Research Fund Denmark (grant no. 7014-00113B/FNU; MSS). This paper is a contribution to the Canada-Germany project ArcTrain supported by NSERC and the NSF-funded Snow on Ice project. Thanks to the two anonymous reviewers who made constructive and useful comments, which helped to improve the manuscript. The authors declare that they have no conflict of interest.

*Author contributions.* – EA, AdV and MSS designed the study. EA carried out the palynological and the carbon isotope analyses and wrote the first draft of the manuscript. AdV and MSS supervised analyses and participated in the overall interpretation of data and editing of the manuscript. MSS was cruise leader of the Sanna 2013 cruise, LM carried out the CTD measurement and analysis, while HR led the sediment coring process during the cruise. JPB validated the linkages with the GIS dynamics. CHM contributed to the interpretation of stable isotope data and supervised the <sup>210</sup>Pb dating of core SA13-ST3-15R. KP picked samples for radiocarbon dating and CP and KP created the age-depth model for core SA13-ST3-20G. LM and HR provided advice

on interpretation. AMM picked samples for stable isotopes, and MTN and JLP performed the grain-size analyses. All co-authors commented on the manuscript.

## References

- Allan, E., de Vernal, A., Knudsen, M. F., Hillaire-Marcel, C., Moros, M., Ribeiro, S., Ouellet-Bernier, M.-M. & Seidenkrantz, M.-S. 2018: Late Holocene sea surface instabilities in the Disko Bugt area, West Greenland, in phase with  $\delta^{18}\text{O}$  oscillations at Camp Century. *Paleoceanography and Paleoclimatology* 33, 227–243.
- Allan, E., de Vernal, A., Krawczyk, D., Moros, M., Radi, T., Rochon, A., Seidenkrantz, M.-S. & Zaragosi, S. 2020: Distribution of dinocyst assemblages in surface sediment samples from the West Greenland margin. *Marine Micropaleontology* 159, 101818, <https://doi.org/10.1016/j.marmicro.2019.101818>.
- Alley, R. & Anandakrishnan, S. 1995: Variations in melt-layer frequency in the GISP2 ice core: implications for Holocene summer temperatures in central Greenland. *Annals of Glaciology* 21, 64–70.
- Alley, R. B., Andrews, J. T., Brigham-Grette, J., Clarke, G. K. C., Cuffey, K. M., Fitzpatrick, J. J., Funder, S., Marshall, S. J., Miller, G. H., Mitrovica, J. X., Muhs, D. R., Otto-Bliesner, B. L., Polyak, L. & White, J. W. C. 2010: History of the Greenland Ice Sheet: paleoclimatic insights. *Quaternary Science Reviews* 29, 1728–1756.
- Andresen, C. S., McCarthy, D. J., Dylmer, C. V., Seidenkrantz, M.-S., Kuijpers, A. & Lloyd, J. M. 2011: Interaction between subsurface ocean waters and calving of the Jakobshavn Isbrae during the late Holocene. *The Holocene* 21, 211–224.
- Assonov, S., Groening, M., Fajgelj, A., Hélie, J. F. & Hillaire-Marcel, C. 2020: Preparation and characterisation of IAEA-603, a new primary reference material aimed at the VPDB scale realisation for  $\delta^{13}\text{C}$  and  $\delta^{18}\text{O}$  determination. *Rapid Communications in Mass Spectrometry* 34, e8867, <https://doi.org/10.1002/rcm.8867>.
- Bennike, O., Wagner, B. & Richter, A. 2011: Relative sea level changes during the Holocene in the Sisimiut area, south-western Greenland. *Journal of Quaternary Science* 26, 353–361.
- Berger, A. & Loutre, M. F. 1991: Insolation values for the climate of the last 10 million years. *Quaternary Science Reviews* 10, 297–317.
- Bilodeau, G., de Vernal, A. & Hillaire-Marcel, C. 1994: Benthic foraminiferal assemblages in Labrador Sea sediments: relations with deep-water mass changes since deglaciation. *Canadian Journal of Earth Sciences* 31, 128–138.
- Boertmann, D., Mosbech, A., Schiedek, D. & Dünweber, M. 2013: Disko West. A strategic environmental impact assessment of hydrocarbon activities. *Scientific Report from DCE – Danish Centre for Environment and Energy No 71*, 306 pp.
- Bonnet, S., de Vernal, A., Hillaire-Marcel, C., Radi, T. & Husum, K. 2010: Variability of sea-surface temperature and sea-ice cover in the Fram Strait over the last two millennia. *Marine Micropaleontology* 74, 59–74.
- ter Braak, C. J. F. & Šmilauer, P. 1998: *Canoco Reference Manual and User's Guide to Canoco for Windows, Software for Canonical Community Ordination (version 4)*. 351 pp. Wageningen, Centre for Biometry.
- ter Braak, C. J. F. & Šmilauer, P. 2012: *Canoco 5: Software for Multivariate Data Exploration, Testing and Summarization. Biometrics*. 362 pp. Plant Research International, The Netherlands.
- Braun, S., Mhatre, S., Jaussi, M., Røy, H., Kjeldsen, K. U., Pearce, C., Seidenkrantz, M.-S., Jørgensen, B. B. & Lomstein, B. 2017: Microbial turnover times in the deep seabed studied by amino acid racemization modelling. *Scientific Reports* 7, 5680, <https://doi.org/10.1038/s41598-017-05972-z>.
- Briner, J. P., McKay, N. P., Axford, Y., Bennike, O., Bradley, R. S., de Vernal, A., Fisher, D., Francus, P., Fréchet, B., Gajewski, K., Jennings, A., Kaufman, D. S., Miller, G., Rouston, C. & Wagner, B. 2016: Holocene climate change in Arctic Canada and Greenland. *Quaternary Science Reviews* 147, 340–364.
- Briner, J. P., Cuzzone, J. K., Badgley, J., Young, N. E., Steig, E. J., Morlighem, M., Schlegel, N., Hakim, G. J., Schaefer, J., Johnson, J. V., Lesnek, A. J., Thomas, E. K., Allan, E., Bennike, O., Cluett, A.,

- Csatho, B. M., de Vernal, A., Downs, J., Larour, E. Y. & Nowicki, S. 2020: Greenland Ice Sheet mass loss rate will exceed Holocene values this century. *Nature* 586, 70–74.
- Bronk Ramsey, C. 2008: Deposition models for chronological records. *Quaternary Science Reviews* 27, 42–60.
- Bronk Ramsey, C. 2009: Bayesian analysis of radiocarbon dates. *Radiocarbon* 51, 337–360.
- Buch, E. 1981: A review of the oceanographic conditions in subarea O and I in the decade 1970–79. NAFO Symposium on Environmental Conditions in the Northwest Atlantic during 1970–79. *NAFO Scientific Council Studies no. 5*, 43–50.
- Caron, M., Rochon, A., Montero-Serrano, J. C. & St-Onge, G. 2019: Evolution of sea-surface conditions on the northwestern Greenland margin during the Holocene. *Journal of Quaternary Science* 34, 569–580.
- Croudace, I. W., Rindby, A. & Rothwell, R. G. 2006: ITRAX: description and evaluation of a new multi-function X-ray core scanner. *Geological Society, London, Special Publications* 267, 51 pp.
- Cuzzone, J. K., Schlegel, N.-J., Morlighem, M., Larour, E., Briner, J. P., Seroussi, H. & Caron, L. 2019: The impact of model resolution on the simulated Holocene retreat of the southwestern Greenland ice sheet using the Ice Sheet System Model (ISSM). *The Cryosphere* 13, 879–893.
- D'Andrea, W. J., Huang, Y., Fritz, S. C. & Anderson, N. J. 2011: Abrupt Holocene climate change as an important factor for human migration in west Greenland. *Proceedings of the National Academy of Sciences of the United States of America* 108, 9765–9769.
- Dale, B. 1996: Dinoflagellate cyst ecology: modeling and geological applications. *Palynology: Principles and Applications* 3, 1249–1275.
- Dowdeswell, J. A., Canals, M., Jakobsson, M., Todd, B. J., Dowdeswell, E. K. & Hogan, K. A. 2016: The variety and distribution of submarine glacial landforms and implications for ice-sheet reconstruction. *Geological Society, London, Memoirs* 46, 519–552.
- Fréchette, B. & de Vernal, A. 2009: Relationship between Holocene climate variations over southern Greenland and eastern Baffin Island and synoptic circulation pattern. *Climate of the Past* 5, 347–359.
- Funder, S., Kjeldsen, K. K., Kjær, K. H. & Ó Cofaigh, C. 2011: The Greenland ice sheet during the last 300,000 years: a review. *Developments in Quaternary Sciences* 15, 699–713.
- Gibb, O. T., Hillaire-Marcel, C. & de Vernal, A. 2014: Oceanographic regimes in the northwest Labrador Sea since Marine Isotope Stage 3 based on dinocyst and stable isotope proxy records. *Quaternary Science Reviews* 92, 269–279.
- Gibb, O. T., Steinhauer, S., Fréchette, B., de Vernal, A. & Hillaire-Marcel, C. 2015: Diachronous evolution of sea surface conditions in the Labrador Sea and Baffin Bay since the last deglaciation. *The Holocene* 25, 1882–1897.
- Glombitza, C., Jaussi, M., Røy, H., Seidenkrantz, M.-S., Lomstein, B. A. & Jørgensen, B. B. 2015: Formate, acetate and propionate as substrates for sulfate reduction in sub-arctic sediments of Southwest Greenland. *Frontiers in Microbiology* 6, 846, <https://doi.org/10.3389/fmicb.2015.00846>.
- Golledge, N. R., Keller, E. D., Gomez, N., Naughten, K. A., Bernales, J., Trusel, L. D. & Edwards, T. L. 2019: Global environmental consequences of twenty-first-century ice-sheet melt. *Nature* 566, 65–72.
- Guiot, J. & de Vernal, A. 2007: Transferfunctions: methods for quantitative paleoceanography based on microfossils. In Hillaire-Marcel, C. & de Vernal, A. (eds.): *Proxies in Late Cenozoic Paleoceanography*, 523–563. Elsevier, Montreal.
- Guiot, J. & de Vernal, A. 2011: Is spatial autocorrelation introducing biases in the apparent accuracy of paleoclimatic reconstructions? *Quaternary Science Reviews* 30, 1965–1972.
- Hanna, E., Jones, J. M., Cappelen, J., Mernild, S. H., Wood, L., Steffen, K. & Huybrechts, P. 2013: The influence of North Atlantic atmospheric and oceanic forcing effects on 1900–2010 Greenland summer climate and ice melt/runoff. *International Journal of Climatology* 33, 862–880.
- Heikkilä, M., Pospelova, V., Forest, A., Stern, G. A., Fortier, L. & Macdonald, R. W. 2016: Dinoflagellate cyst production over an annual cycle in seasonally ice-covered Hudson Bay. *Marine Micropaleontology* 125, 1–24.
- Heikkilä, M., Pospelova, V., Hochheim, K. P., Kuzyk, Z. Z. A., Stern, G. A., Barber, D. G. & Macdonald, R. W. 2014: Surface sediment dinoflagellate cysts from the Hudson Bay system and their relation to freshwater and nutrient cycling. *Marine Micropaleontology* 106, 79–109.
- Hillaire-Marcel, C., de Vernal, A., Bilodeau, G. & Weaver, A. J. 2001: Absence of deep-water formation in the Labrador Sea during the Last Interglacial period. *Nature* 410, 1073–1077.
- Hohmann, S., Kucera, M. & de Vernal, A. 2020: Identifying the signature of sea-surface properties in dinocyst assemblages: implications for quantitative palaeoceanographical reconstructions by transfer functions and analogue techniques. *Marine Micropaleontology* 159, 101816, <https://doi.org/10.1016/j.marmicro.2019.101816>.
- Hoogakker, B. A. A., McCave, I. N., Elderfield, H., Hillaire-Marcel, C. & Simstich, J. 2015: Holocene climate variability in the Labrador Sea. *Journal of the Geological Society* 172, 272–277.
- Jackson, L. C., Peterson, K. A., Roberts, C. D. & Wood, R. A. 2016: Recent slowing of Atlantic overturning circulation as a recovery from earlier strengthening. *Nature Geoscience* 9, 518–522.
- Jennings, A. E., Andrews, J. T., Ó Cofaigh, C., Onge, G. S., Sheldon, C., Belt, S. T., Cabedo-Sanz, P. & Hillaire-Marcel, C. 2017: Ocean forcing of Ice Sheet retreat in central west Greenland from LGM to the early Holocene. *Earth and Planetary Science Letters* 472, 1–13.
- Jennings, A. E., Walton, M. E., Ó Cofaigh, C., Kilfeather, A., Andrews, J. T., Ortiz, J. D., de Vernal, A. & Dowdeswell, J. A. 2014: Paleoenvironments during Younger Dryas–Early Holocene retreat of the Greenland Ice Sheet from outer Disko Trough, central west Greenland. *Journal of Quaternary Science* 29, 27–40.
- Jensen, J. F. 2006: Stone age of Qeqertarsuup Tunua (Disko Bugt): A regional analysis of the Saqqaq and Dorset cultures of central west Greenland. *Monographs on Greenland, Man & Society* 32, 272 pp.
- Juggins, S. 2013: Quantitative reconstructions in palaeolimnology: new paradigm or sick science? *Quaternary Science Reviews* 54, 20–32.
- Juggins, S. & Birks, H. J. B. 2012: Quantitative environmental reconstructions from biological data. In Smol, J., Birks, H. J. B. & Last, W. M. (eds): *Tracking Environmental Change Using Lake Sediments*, 431–494. Springer, Dordrecht.
- Juul-Pedersen, T., Arendt, K. E., Mortensen, J., Blicher, M. E., Søgaard, D. H. & Rysgaard, S. 2015: Seasonal and interannual phytoplankton production in a sub-Arctic tidewater outlet glacier fjord, SW Greenland. *Marine Ecology Progress Series* 524, 27–38.
- Knudsen, K. L., Stabell, B., Seidenkrantz, M.-S., Eiriksson, J. & Blake Jr, W. 2008: Deglacial and Holocene conditions in northernmost Baffin Bay: sediments, foraminifera, diatoms and stable isotopes. *Boreas* 37, 346–376.
- Kobashi, T., Menviel, L., Jeltsch-Thömmes, A., Vinther, B. M., Box, J. E., Muscheler, R., Nakaegawa, T., Pfister, P. L., Döring, M., Leuenberger, M., Wanner, H. & Ohmura, A. 2017: Volcanic influence on centennial to millennial Holocene Greenland temperature change. *Scientific Reports* 7, 1441, <https://doi.org/10.1038/s41598-017-01451-7>.
- Kolling, H. M., Stein, R., Fahl, K., Perner, K. & Moros, M. 2017: Short-term variability in late Holocene sea ice cover on the East Greenland Shelf and its driving mechanisms. *Palaeogeography, Palaeoclimatology, Palaeoecology* 485, 336–350.
- Korsun, S. & Hald, M. 2000: Seasonal dynamics of benthic foraminifera in a glacially fed fjord of Svalbard, European Arctic. *Journal of Foraminiferal Research* 30, 251–271.
- Krawczyk, D. W., Kryk, A., Juggins, S., Burmeister, A., Pearce, C., Seidenkrantz, M.-S., Moros, M., Hoyer, J. L., Kuijpers, A. & Witkowski, A. 2021: Spatio-temporal changes in ocean conditions and primary production in Baffin Bay and the Labrador Sea. *Palaeogeography, Palaeoclimatology, Palaeoecology* 563, 110175, <https://doi.org/10.1016/j.palaeo.2020.110175>.
- Krawczyk, D. W., Meire, L., Lopes, C., Juul-Pedersen, T., Mortensen, J., Li, C. L. & Krogh, T. 2018: Seasonal succession, distribution, and diversity of planktonic protists in relation to hydrography of the Godthåbsfjord system (SW Greenland). *Polar Biology* 41, 2033–2052.
- Krawczyk, D. W., Witkowski, A., Juul-Pedersen, T., Arendt, K. E., Mortensen, J. & Rysgaard, S. 2015: Microplankton succession in a

- SW Greenland tidewater glacial fjord influenced by coastal inflows and run-off from the Greenland ice sheet. *Polar Biology* 38, 1515–1533.
- Krawczyk, D. W., Witkowski, A., Lloyd, J., Moros, M., Harff, J. & Kuijpers, A. 2013: Late-Holocene diatom derived seasonal variability in hydrological conditions off Disko Bay, West Greenland. *Quaternary Science Reviews* 67, 93–104.
- Krawczyk, D. W., Witkowski, A., Moros, M., Lloyd, J. M., Høyer, J. L., Miettinen, A. & Kuijpers, A. 2017: Quantitative reconstruction of Holocene sea ice and sea surface temperature off West Greenland from the first regional diatom data set. *Paleoceanography* 32, 18–40.
- Krawczyk, D., Witkowski, A., Moros, M., Lloyd, J., Kuijpers, A. & Kierzek, A. 2010: Late-Holocene diatom-inferred reconstruction of temperature variations of the West Greenland current from Disko Bugt, central West Greenland. *The Holocene* 20, 659–666.
- Larsen, N. K., Funder, S., Kjær, K. H., Kjeldsen, K. K., Knudsen, M. F. & Linge, H. 2014: Rapid early Holocene ice retreat in West Greenland. *Quaternary Science Reviews* 92, 310–323.
- Larsen, N. K., Kjær, K. H., Lecavalier, B., Bjørk, A. A., Colding, S., Huybrechts, P., Jakobsen, K. E., Kjeldsen, K. K., Knudsen, K.-L., Odgaard, B. V. & Olsen, J. 2015: The response of the southern Greenland ice sheet to the Holocene thermal maximum. *Geology* 43, 291–294.
- Larsen, N. K., Strunk, A., Levy, L. B., Olsen, J., Bjørk, A., Lauridsen, T. L., Jeppesen, E. & Davidson, T. A. 2017: Strong altitudinal control on the response of local glaciers to Holocene climate change in southwest Greenland. *Quaternary Science Reviews* 168, 69–78.
- Lecavalier, B. S., Milne, G. A., Simpson, M. J., Wake, L., Huybrechts, P., Tarasov, L., Kjeldsen, K. K., Funder, S., Long, A. J., Woodroffe, S., Dyke, A. S. & Larsen, N. K. 2014: A model of Greenland ice sheet deglaciation constrained by observations of relative sea level and ice extent. *Quaternary Science Reviews* 102, 54–84.
- Legendre, P. & Birks, H. J. B. 2012: From classical to canonical ordination. In Smol, J., Birks, H. J. B. & Last, W. M. (eds.): *Tracking Environmental Change Using Lake Sediments*, 201–248. Springer, Dordrecht.
- Legendre, P. & Legendre, L. 2012: *Numerical Ecology*. 990 pp. Elsevier Science BV, Amsterdam.
- Lepš, J. & Šmilauer, P. 2014: *Multivariate Analysis of Ecological Data Using Canoco 5*. 362 pp. Cambridge University Press, Cambridge.
- Lesnek, A. J., Briner, J. P., Young, N. E. & Cuzzone, J. K. 2020: Maximum Southwest Greenland ice sheet recession in the early Holocene. *Geophysical Research Letters* 47, e2019GL083164. <https://doi.org/10.1029/2019GL083164>.
- Levac, E., de Vernal, A., & Blake Jr, W. 2001: Sea-surface conditions in northernmost Baffin Bay during the Holocene: Palynological evidence. *Journal of Quaternary Science: Published for the Quaternary Research Association* 16, 353–363.
- Levy, L. B., Larsen, N. K., Davidson, T. A., Strunk, A., Olsen, J. & Jeppesen, E. 2017: Contrasting evidence of Holocene ice margin retreat, south-western Greenland. *Journal of Quaternary Science* 32, 604–616.
- Lloyd, J. M., Kuijpers, A., Long, A., Moros, M. & Park, L. A. 2007: Foraminiferal reconstruction of mid- to late-Holocene ocean circulation and climate variability in Disko Bugt, West Greenland. *The Holocene* 17, 1079–1091.
- Lloyd, J., Moros, M., Perner, K., Telford, R. J., Kuijpers, A., Jansen, E. & McCarthy, D. 2011: A 100 yr record of ocean temperature control on the stability of Jakobshavn Isbrae, West Greenland. *Geology* 39, 867–870.
- Long, A. J., Woodroffe, S. A., Dawson, S., Roberts, D. H. & Bryant, C. L. 2009: Late Holocene relative sea level rise and the Neoglacial history of the Greenland ice sheet. *Journal of Quaternary Science* 24, 345–359.
- Long, A. J., Woodroffe, S. A., Roberts, D. H. & Dawson, S. 2011: Isolation basins, sea-level changes and the Holocene history of the Greenland Ice Sheet. *Quaternary Science Reviews* 30, 3748–3768.
- McGhee, R. 1996: *Ancient People of the Arctic*. 244 pp. UCB Press, Vancouver.
- McGovern, T. 1991: Climate correlation and causation in Norse Greenland. *Arctic Anthropology* 28, 77–100.
- Meire, L., Meire, P., Struyf, E., Krawczyk, D. W., Arendt, K. E., Yde, J. C., Juul Pedersen, T., Hopwood, M. J., Rysgaard, S. & Meysman, F. J. R. 2016: High export of dissolved silica from the Greenland ice sheet. *Geophysical Research Letters* 43, 9173–9182.
- Meire, L., Mortensen, J., Meire, P., Juul-Pedersen, T., Sejr, M. K., Rysgaard, S., Nygaard, R., Huybrechts, P. & Meysman, F. J. R. 2017: Marine-terminating glaciers sustain high productivity in Greenland fjords. *Global Change Biology* 23, 5344–5357.
- Mertens, K. N., Verhoeven, K., Verleye, T., Louwye, S., Amorim, A., Ribeiro, S., Deaf, A. S., Harding, I. C., De Schepper, S., González, C., Kodrans-Nsiah, M., de Vernal, A., Henry, M., Radi, T., Dybkjaer, K., Poulsen, N. E., Feist-Burkhardt, S., Chitolie, J., Heilmann-Clausen, C., Londeix, L., Turon, J.-L., Marret, F., Matthiessen, J., McCarthy, F. M. G., Prasad, V., Pospelova, V., Kyffin Hughes, J. E., Riding, J. B., Rochon, A., Sangiorgi, F., Welters, N., Sinclair, N., Thun, C., Soliman, A., Van Nieuwenhove, N., Vink, A. & Young, M. 2009: Determining the absolute abundance of dinoflagellate cysts in recent marine sediments: the *Lycopodium* marker-grain method put to the test. *Review of Palaeobotany and Palynology* 157, 238–252.
- Meyers, P. A. 1994: Preservation of elemental and isotopic source identification of sedimentary organic matter. *Chemical Geology* 114, 289–302.
- Meyers, P. A. 1997: Organic geochemical proxies of paleoceanographic, paleolimnologic, and paleoclimatic processes. *Organic Geochemistry* 27, 213–250.
- Møller, H. S., Jensen, K. G., Kuijpers, A., Aagaard-Sørensen, S., Seidenkrantz, M.-S., Prins, M., Endler, R. & Mikkelsen, N. 2006: Late-Holocene environment and climatic changes in Ameralik Fjord, southwest Greenland: evidence from the sedimentary record. *The Holocene* 16, 685–695.
- Moros, M., Jensen, K. G. & Kuijpers, A. 2006: Mid- to late-Holocene hydrological and climatic variability in Disko Bugt, central West Greenland. *The Holocene* 16, 357–367.
- Moros, M., Lloyd, J. M., Perner, K., Krawczyk, D., Blanz, T., de Vernal, A., Ouellet-Bernier, M.-M., Kuijpers, A., Jennings, A. E., Witkowski, A., Schneider, R. & Jansen, E. 2016: Surface and sub-surface multiproxy reconstruction of middle to late Holocene paleoceanographic changes in Disko Bugt, West Greenland. *Quaternary Science Reviews* 132, 146–160.
- Mortensen, J., Bendtsen, J., Lennert, K. & Rysgaard, S. 2014: Seasonal variability of the circulation system in a west Greenland tidewater outlet glacier fjord, Godthåbsfjord (64 N). *Journal of Geophysical Research: Earth Surface* 119, 2591–2603.
- Mortensen, J., Lennert, K., Bendtsen, J. & Rysgaard, S. 2011: Heat sources for glacial melt in a sub-Arctic fjord (Godthåbsfjord) in contact with the Greenland Ice Sheet. *Journal of Geophysical Research: Oceans* 116, C01013, <https://doi.org/10.1029/2010JC006528>.
- Muzuka, A. N. & Hillaire-Marcel, C. 1999: Burial rates of organic matter along the eastern Canadian margin and stable isotope constraints on its origin and diagenetic evolution. *Marine Geology* 160, 251–270.
- Nørgaard-Pedersen, N. & Mikkelsen, N. 2009: 8000 year marine record of climate variability and fjord dynamics from Southern Greenland. *Marine Geology* 264, 177–189.
- Ó Cofaigh, C., Dowdeswell, J. A., Jennings, A. E., Hogan, K. A., Kilfeather, K., Hiemstra, J. F., Noormets, R., Evans, J., McCarthy, D. J., Andrews, J. T., Lloyd, J. M. & Moros, M. 2013: An extensive and dynamic ice sheet on the West Greenland shelf during the last glacial cycle. *Geology* 41, 219–222.
- Ólafsdóttir, S., Jennings, A. E., Geirsdóttir, Á., Andrews, J. & Miller, G. H. 2010: Holocene variability of the North Atlantic Irminger current on the south- and northwest shelf of Iceland. *Marine Micropaleontology* 77, 101–118.
- Ouellet-Bernier, M.-M., de Vernal, A., Hillaire-Marcel, C. & Moros, M. 2014: Paleoceanographic changes in the Disko Bugt area, West Greenland, during the Holocene. *The Holocene* 24, 1573–1583.
- Pearce, D. M., Mair, D. W., Rea, B. R., Lea, J. M., Schofield, J. E., Kamenos, N. & Schoenrock, K. 2018: The glacial geomorphology of upper Godthåbsfjord (Nuup Kangerlua) in southwest Greenland. *Journal of Maps* 14, 45–55.

- Pearce, C., Seidenkrantz, M.-S., Kuijpers, A. & Reynisson, N. F. 2014: A multi-proxy reconstruction of oceanographic conditions around the Younger Dryas-Holocene transition in Placentia Bay, Newfoundland. *Marine Micropaleontology* 112, 39–49.
- Pelikan, C., Jaussi, M., Wasmund, K., Seidenkrantz, M.-S., Pearce, C., Kuzyk, Z. Z. A., Herbold, C. W., Røy, H., Keldsen, K. U. & Loy, A. 2019: Glacial runoff promotes deep burial of sulfur cycling-associated microorganisms in marine sediments. *Frontiers in Microbiology* 10, 2558–2558.
- Perner, K., Moros, M., Jennings, A., Lloyd, J. M. & Knudsen, K. L. 2013: Holocene palaeoceanographic evolution off west Greenland. *The Holocene* 23, 374–387.
- Perner, K., Moros, M., Lloyd, J. M., Kuijpers, A., Telford, R. J. & Harff, J. 2011: Centennial scale benthic foraminiferal record of late Holocene oceanographic variability in Disko Bugt, West Greenland. *Quaternary Science Reviews* 30, 2815–2826.
- Peyron, O. & de Vernal, A. 2001: Application of artificial neural networks (ANN) to high-latitude dinocyst assemblages for the reconstruction of past sea-surface conditions in Arctic and sub-Arctic seas. *Journal of Quaternary Science* 16, 699–709.
- Radi, T. & de Vernal, A. 2008: Dinocysts as proxy of primary productivity in mid-high latitudes of the Northern Hemisphere. *Marine Micropaleontology* 68, 84–114.
- Radi, T., Bonnet, S., Cormier, M.-A., de Vernal, A., Durantou, L., Faubert, É., Head, M. J., Henry, M., Pospelova, V., Rochon, A. & Van Nieuwenhove, N. 2013: Operational taxonomy and (paleo-)jauteology of round, brown, spiny dinoflagellate cysts from the Quaternary of high northern latitudes. *Marine Micropaleontology* 98, 41–57.
- Rahmstorf, S., Box, J. E., Feulner, G., Mann, M. E., Robinson, A., Rutherford, S. & Schaffernicht, E. J. 2015: Exceptional twentieth-century slowdown in Atlantic Ocean overturning circulation. *Nature Climate Change* 5, 475–480.
- Reimer, P. J. & Reimer, R. W. 2001: A marine reservoir correction database and on-line interface. *Radiocarbon* 43, 461–463.
- Ren, J., Jiang, H., Seidenkrantz, M.-S. & Kuijpers, A. 2009: A diatom-based reconstruction of Early Holocene hydrographic and climatic change in a southwest Greenland fjord. *Marine Micropaleontology* 70, 166–176.
- Ribeiro, S., Moros, M., Ellegaard, M. & Kuijpers, A. 2012: Climate variability in West Greenland during the past 1500 years: evidence from a high-resolution marine palynological record from Disko Bay. *Boreas* 41, 68–83.
- Ribergaard, M. H. 2014: *Oceanographic Investigations off West Greenland 2013*. NAFO Scientific Council Documents, Dartmouth, Nova Scotia, Canada.
- Rignot, E., Koppes, M. & Velicogna, I. 2010: Rapid submarine melting of the calving faces of West Greenland glaciers. *Nature Geoscience* 3, 187–191.
- Rochon, A., de Vernal, A., Turon, J.-L., Matthiessen, J. & Head, M. J. 1999: Distribution of recent dinoflagellate cysts in surface sediments from the North Atlantic Ocean and adjacent seas in relation to sea surface parameters. *American Association of Stratigraphic Palynologists Contribution Series* 35, 1–146.
- Rothwell, R. G. & Croudace, I. W. 2015: Twenty years of XRF core scanning marine sediments: what do geochemical proxies tell us? In Croudace, I. W. & Rothwell, R. G. (eds.): *Micro-XRF Studies of Sediment Cores*, 25–102. Springer, Dordrecht.
- Ryan, J. C., Dowdeswell, J. A. & Hogan, K. A. 2016: Three cross-shelf troughs on the continental shelf of SW Greenland from Olex data. *Geological Society, London, Memoirs* 46, 167–168.
- Rysgaard, S., Boone, W., Carlson, D., Sej, M. K., Bendtsen, J., Juul-Pedersen, T., Lund, H., Meire, L. & Mortensen, J. 2020: An updated view on water masses on the pan-West Greenland Continental Shelf and their link to proglacial fjords. *Journal of Geophysical Research: Oceans* 125, e2019JC015564, <https://doi.org/10.1029/2019JC015564>.
- Schweinsberg, A. D., Briner, J. P., Miller, G. H., Bennike, O. & Thomas, E. K. 2017: Local glaciation in West Greenland linked to North Atlantic Ocean circulation during the Holocene. *Geology* 45, 195–198.
- Schweinsberg, A. D., Briner, J. P., Miller, G. H., Lifton, N. A., Bennike, O. & Graham, B. L. 2018: Holocene mountain glacier history in the Sukkertoppen Iskappe area, southwest Greenland. *Quaternary Science Reviews* 197, 142–161.
- Seidenkrantz, M.-S., Aagaard-Sørensen, S., Sulsbrück, H., Kuijpers, A., Jensen, K. G. & Kunzendorf, H. 2007: Hydrography and climate of the last 4400 years in a SW Greenland fjord: implications for Labrador Sea palaeoceanography. *The Holocene* 17, 387–401.
- Seidenkrantz, M.-S., Ebbesen, H., Aagaard-Sørensen, S., Moros, M., Lloyd, J. M., Olsen, J., Knudsen, M. F. & Kuijpers, A. 2013a: Early Holocene large-scale meltwater discharge from Greenland documented by foraminifera and sediment parameters. *Palaeogeography, Palaeoclimatology, Palaeoecology* 391, Part A, 71–81.
- Seidenkrantz, M.-S., Roncaglia, L., Fischel, A., Heilmann-Clausen, C., Kuijpers, A. & Moros, M. 2008: Variable North Atlantic climate seesaw patterns documented by a late Holocene marine record from Disko Bugt, West Greenland. *Marine Micropaleontology* 68, 66–83.
- Seidenkrantz, M.-S., Røy, H., Lomstein, B. A., Meire, L. & the shipboard and on-shore parties 2013b: *Godthåbsfjord system and the West Greenland shelf with 'RIV Sanna', 11–16. August 2013*. Cruise report, Aarhus University.
- Seidenkrantz, M.-S., Kuijpers, A., Olsen, J., Pearce, C., Lindblom, S., Ploug, J., Przybylo, P. & Snowball, I. 2019: Southwest Greenland shelf glaciation during MIS 4 more extensive than during the Last Glacial Maximum. *Scientific Reports*, 9, 1–11.
- Sévellec, F., Fedorov, A. V. & Liu, W. 2017: Arctic sea-ice decline weakens the Atlantic Meridional Overturning Circulation. *Nature Climate Change* 7, 604–610.
- Sha, L., Jiang, H., Seidenkrantz, M.-S., Knudsen, K. L., Olsen, J., Kuijpers, A. & Liu, Y. 2014: A diatom-based sea-ice reconstruction for the Vaigat Strait (Disko Bugt, West Greenland) over the last 5000 yr. *Palaeogeography, Palaeoclimatology, Palaeoecology* 403, 66–79.
- Shapiro, S. S. & Wilk, M. B. 1965: An analysis of variance test for normality (complete samples). *Biometrika* 52, 591–611.
- Sheldon, C., Jennings, A., Andrews, J. T., Ó Cofaigh, C., Hogan, K., Dowdeswell, J. A. & Seidenkrantz, M.-S. 2016: Ice stream retreat following the LGM and onset of the west Greenland current in Uummannaq Trough, west Greenland. *Quaternary Science Reviews* 147, 27–46.
- Smith, J. N. & Schafer, C. T. 1984: Bioturbation processes in continental slope and rise sediments delineated by Pb-210, microfossil and textural indicators. *Journal of Marine Research* 42, 1117–1145.
- Solignac, S., Seidenkrantz, M.-S., Jessen, C., Kuijpers, A., Gunvald, A. K. & Olsen, J. 2011: Late-Holocene sea-surface conditions offshore Newfoundland based on dinoflagellate cysts. *The Holocene* 21, 539–552.
- Solignac, S., de Vernal, A. & Hillaire-Marcel, C. 2004: Holocene sea-surface conditions in the North Atlantic—contrasted trends and regimes in the western and eastern sectors (Labrador Sea vs. Iceland Basin). *Quaternary Science Reviews* 23, 319–334.
- Sparrenbom, C. J., Bennike, O., Björck, S. & Lambeck, K. 2006: Relative sea-level changes since 15 000 cal. yr BP in the Nanortalik area, southern Greenland. *Journal of Quaternary Science* 21, 29–48.
- St-Onge, G., Mulder, T., Francus, P. & Long, B. 2007: Continuous physical properties of cored marine sediments. In Hillaire-Marcel, C. & de Vernal, A. (eds.): *Proxies in Late Cenozoic Paleooceanography*, 63–98. Elsevier, Amsterdam.
- Tang, C. C. L., Ross, C. K., Yao, T., Petrie, B., DeTracey, B. M. & Dunlap, E. 2004: The circulation, water masses and sea-ice of Baffin Bay. *Progress in Oceanography* 63, 183–228.
- Tremblay, J., Anderson, L. G., Matrai, P., Coupel, P., Bélanger, S., Michel, C. & Reigstad, M. 2015: Global and regional drivers of nutrient supply, primary production and CO<sub>2</sub> drawdown in the changing Arctic ocean. *Progress in Oceanography* 139, 171–196.
- Van Nieuwenhove, N., Head, M. J., Limoges, A., Pospelova, V., Mertens, K. N., Matthiessen, J., De Schepper, S., de Vernal, A., Eynaud, F., Londeix, L., Marret, F., Penaud, A., Radi, T. & Rochon, A. 2020: An overview and brief description of common marine organic-walled dinoflagellate cyst taxa occurring in surface sediments of the Northern Hemisphere. *Marine Micropaleontology* 159, 101814, <https://doi.org/10.1016/j.marmicro.2019.101814>.
- de Vernal, A. & Hillaire-Marcel, C. 2006: Provincialism in trends and high frequency changes in the northwest North Atlantic during the Holocene. *Global and Planetary Change* 54, 263–290.

- de Vernal, A., Henry, M. & Bilodeau, G. 1996: Techniques de préparation et d'analyses en micropaléontologie. *Les cahiers du GEOTOP* 3, 16–24.
- de Vernal, A., Henry, M., Matthiessen, J., Mudie, P. J., Rochon, A., Boessenkool, K. P., Eynaud, F., Grösfeld, K., Guiot, J., Hamel, D., Harland, R., Head, M. J., Kunz-Pirrung, M., Levac, E., Loucheur, V., Peyron, O., Pospelova, V., Radi, T., Turon, J.-L. & Voronina, E. 2001: Dinoflagellate cyst assemblages as tracers of sea-surface conditions in the northern North Atlantic, Arctic and sub-Arctic seas: The new 'n = 677' data base and its application for quantitative palaeoceanographic reconstruction. *Journal of Quaternary Science* 16, 681–698.
- de Vernal, A., Radi, T., Zaragosi, S., Van Nieuwenhove, N., Rochon, A., Allan, E., De Schepper, S., Eynaud, F., Head, M., Limoges, A., Londeix, L., Marret-Davies, F., Matthiessen, J., Penaud, A., Pospelova, V., Price, A. & Richerol, T. 2020: Distribution of common modern dinocyst taxa in surface sediments of the Northern Hemisphere in relation to environmental parameters: the updated n=1968 database. *Marine Micropaleontology* 159, 101796, <https://doi.org/10.1016/j.marmicro.2019.101796>.
- de Vernal, A., Rochon, A., Fréchette, B., Henry, M., Radi, T. & Solignac, S. 2013: Reconstructing past sea ice cover of the Northern Hemisphere from dinocyst assemblages: status of the approach. *Quaternary Science Reviews* 79, 122–134.
- Vinther, B. M., Buchardt, S. L., Clausen, H. B., Dahl-Jensen, D., Johnsen, S. J., Fisher, D. A., Koerner, R. M., Raynaud, D., Lipenkov, V., Andersen, K. K., Blunier, T., Rasmussen, S. O., Steffensen, J. P. & Svensson, A. M. 2009: Holocene thinning of the Greenland Ice Sheet. *Nature* 461, 385–388.
- Young, N. E. & Briner, J. P. 2015: Holocene evolution of the western Greenland Ice Sheet: assessing geophysical ice-sheet models with geological reconstructions of ice-margin change. *Quaternary Science Reviews* 114, 1–17.
- Young, N. E., Briner, J. P., Miller, G. H., Lesnek, A. J., Crump, S. E., Thomas, E. K., Pendleton, S. L., Cuzzone, J., Lamp, J., Zimmerman, S., Caffee, M. & Schaefer, J. M. 2020: Deglaciation of the Greenland and Laurentide ice sheets interrupted by glacier advance during abrupt coolings. *Quaternary Science Reviews* 229, 106091, <https://doi.org/10.1016/j.quascirev.2019.106091>.
- Zonneveld, K. A., Versteegh, G. & Kodrans-Nsiah, M. 2008: Preservation and organic chemistry of Late Cenozoic organic-walled dinoflagellate cysts: a review. *Marine Micropaleontology* 68, 179–197.
- Zonneveld, K. A., Versteegh, G. J. & de Lange, G. J. 2001: Palaeoproductivity and post-depositional aerobic organic matter decay reflected by dinoflagellate cyst assemblages of the Eastern Mediterranean S1 sapropel. *Marine Geology* 172, 181–195.

## Supporting Information

Additional Supporting Information may be found in the online version of this article at <http://www.boreas.dk>.

*Fig. S1.* Percentage of organic carbon ( $C_{\text{org}}$ ) inorganic carbon ( $C_{\text{inorg}}$ ) and  $C_{\text{org}}/C_{\text{inorg}}$  ratio.

*Fig. S2.* Percentage of all dinocyst taxa; the red line indicates an exaggeration of  $\times 10$ .

*Table S1.* Results of  $^{210}\text{Pb}$  measurement in Rumohr lot core 15R.

*Table S2.* Results of XRF core scanning and magnetic susceptibility from the Rumohr lot core 16R and results of XRF core scanning, magnetic susceptibility, calcium carbonate and organic carbon content from the core 20G.

*Table S3.* Results of particle size analysis from the core 20G.

*Table S4.* Results of oxygen and carbon isotope composition ( $\delta^{18}\text{O}$ ,  $\delta^{13}\text{C}$ ) of the deep benthic foraminiferal species *Nonionellina labradorica* (Dawson), and carbon isotope composition ( $\delta^{13}\text{C}$ ) of the organic matter from the core 20G.

*Table S5.* Detailed results of dinocyst assemblages (counting, percentages and concentration) and results of MAT.